nature cell biology

During autophagy mitochondria elongate, are spared from degradation and sustain cell viability

Ligia C. Gomes[1,2,3], Giulietta Di Benedetto[2,4] and Luca Scorrano[1,2,5,6]

A plethora of cellular processes, including apoptosis, depend on regulated changes in mitochondrial shape and ultrastructure. The role of mitochondria and of their morphology during autophagy, a bulk degradation and recycling process of eukaryotic cells' constituents, is not well understood. Here we show that mitochondrial morphology determines the cellular response to macroautophagy. When autophagy is triggered, mitochondria elongate *in vitro* and *in vivo*. During starvation, cellular cyclic AMP levels increase and protein kinase A (PKA) is activated. PKA in turn phosphorylates the pro-fission dynamin-related protein 1 (DRP1), which is therefore retained in the cytoplasm, leading to unopposed mitochondrial fusion. Elongated mitochondria are spared from autophagic degradation, possess more cristae, increased levels of dimerization and activity of ATP synthase, and maintain ATP production. Conversely, when elongation is genetically or pharmacologically blocked, mitochondria consume ATP, precipitating starvation-induced death. Thus, regulated changes in mitochondrial morphology determine the fate of the cell during autophagy.

Mitochondria are crucial organelles for energy production, regulation of cell signalling and amplification of apoptosis. This functional versatility is matched by their morphological and structural variety. During the lifetime of a cell, the mitochondrial network is continuously shaped by fission and fusion events[1]. The dynamin-related GTPases optic atrophy 1 (OPA1) of the inner mitochondrial membrane[2], and mitofusins (MFN) 1 and 2 of the outer membrane[3], regulate mitochondrial fusion in mammalian cells. Mitochondrial fission is controlled by cytosolic DRP1 (ref. 4). Translocation of DRP1 to mitochondria is an essential step in the fragmentation of the organelle and depends on dephosphorylation of the Ser 637 residue by calcineurin[5]. Conversely, phosphorylation of Ser 637 by PKA promotes mitochondrial elongation[6,7]. Once on mitochondria, resident small ubiquitin-like modifier (SUMO) ligases, such as mitochondrial-anchored protein ligase[9] (MAPL), can stabilize DRP1 by SUMOylation[8], demonstrating how dynamic regulation of fission adapts mitochondrial morphology to the changing needs of the cell.

The availability of genetic tools has allowed investigation of the role of mitochondrial morphology in complex cellular processes. For example, remodelling of mitochondrial cristae[10] and fragmentation of the organellar network[11,12] participate in the progression of apoptosis. More recently, Ca^{2+} signalling[13], formation of dendritic spines[14], migration of lymphocytes[15], cell cycle[16], and even lifespan in *Podospora anserina* and *Saccharomyces cerevisiae*[17] have been found to depend on regulated changes in mitochondrial morphology. Finally, mitophagy, a particular form of selective autophagy of mitochondria, requires fragmentation of the mitochondrial network to segregate the dysfunctional units to be removed[18,19].

Autophagy is a self-degradation process induced, for example, when nutrients are limited[20]. During autophagy, pre-autophagosomal structures engulf components of the cytosol, including entire organelles, giving rise to autophagosomes that ultimately fuse with lysosomes, where breakdown of cellular components takes place[21]. For many years, autophagy has been regarded as an unselective process, but it is now clear that under certain conditions specific cargoes are selectively targeted to autophagy, including aggregated proteins[22], invading bacteria[23] and superfluous or damaged organelles, such as peroxisomes[24], endoplasmic reticulum membranes[25] and mitochondria[26]. Not only can organelles be selectively eliminated by autophagy, but they also participate in the different steps of macroautophagy, ranging from the formation of the autophagosomal membrane[27], to the amplification of the process, in which mitochondria-derived reactive oxygen species seem to play a role[28]. Mitochondria may also serve as docking sites for the formation of the autophagosomes[29] in a process that depends on the tethering of the mitochondria to the endoplasmic reticulum[30]. However, many questions on the morphology as well as on the functional role of mitochondria during autophagy remain open. For example, it is unclear whether mitochondria fragment,

[1]Dulbecco-Telethon Institute, Via Orus 2, 35129 Padova, Italy. [2]Venetian Institute of Molecular Medicine, Via Orus 2, 35129 Padova, Italy. [3]PhD Programme in Experimental Biology and Biomedicine, Center for Neuroscience and Cell Biology, University of Coimbra, 3004-517 Coimbra, Portugal. [4]CNR Institute for Neurosciences, Section of Padova, Via G. Colombo 3, 35129 Padova, Italy. [5]Department of Cell Physiology and Medicine, University of Geneva, 1 Rue M. Servet, 1211 Geneve, Switzerland.
[6]Correspondence should be addressed to L.S. (e-mail: luca.scorrano@unige.ch)

Received 24 May 2010; accepted 31 January 2011; published online 10 April 2011; DOI: 10.1038/ncb2220

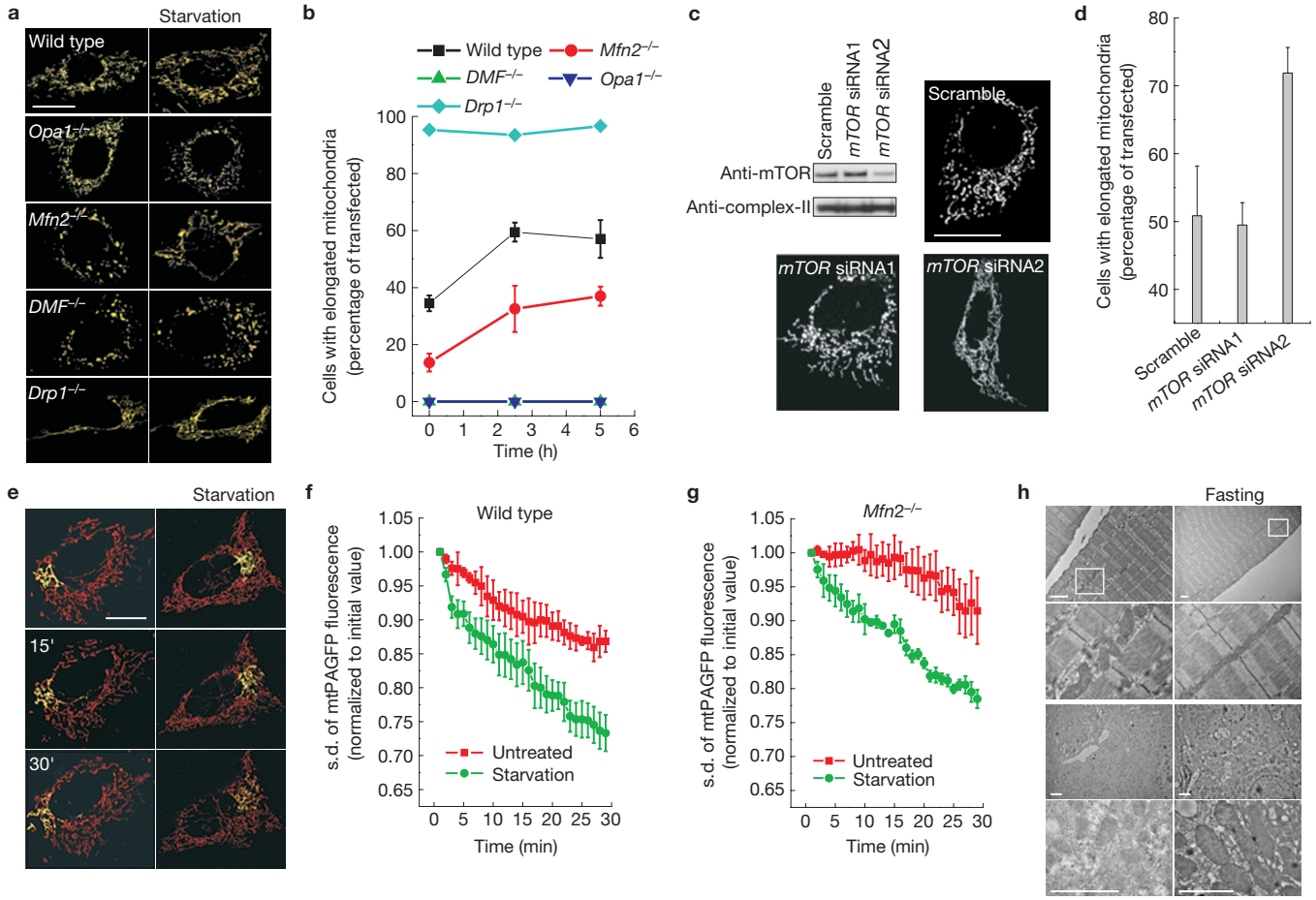

Figure 1 Mitochondrial elongation in response to autophagy. (**a**) Representative confocal micrographs of mitochondrial morphology in MEFs of the indicated genotype 24 h after transfection with mtYFP. Where indicated, cells were starved for 2.5 h. Scale bar, 20 μm. (**b**) Morphometric analysis of mitochondrial shape. Experiments were carried out as in **a**. Data represent mean ± s.e.m. of three independent experiments ($n = 100$ cells per condition in each experiment). (**c**) Top left, 48 h after transfection with the indicated siRNA, MEFs were lysed and 25 μg samples of proteins were separated by SDS–polyacrylamide gel electrophoresis (PAGE) and immunoblotted with the indicated antibodies. Top right and bottom, representative images show mitochondrial morphology of MEFs transfected with the indicated siRNA and after 24 h with mtYFP. After a further 24 h, confocal micrographs were acquired. Scale bar, 20 μm. Uncropped images of blots are shown in Supplementary Fig. S8. (**d**) Morphometric analysis of mitochondrial shape. Experiments were carried out as in **c**. Data represent mean ± s.e.m. of five independent experiments ($n = 100$ cells per condition in each experiment). (**e**) Representative images of mitochondrial fusion over time (indicated in min). MEFs were co-transfected with mtPAGFP and mtRFP and after 24 h, mtPAGFP was photoactivated in a region of interest and cells were imaged by real-time confocal microscopy. Where indicated, MEFs were starved for 2.5 h. Scale bar, 20 μm. See also Supplementary Movies S1 and S2. (**f**,**g**) Quantification of mitochondrial fusion in MEFs of the indicated genotype. Experiments were carried out as in **e**. Data represent mean ± s.e.m. of four independent experiments. (**h**) Representative electron micrographs of muscle (longitudinal sections; four top micrographs) and liver (four bottom micrographs) from CD1 mice. Where indicated, mice were fasted for 12 h. The outlined regions of micrographs from muscle samples are magnified ×7 in the images below. Scale bars, 2 μm.

if they are randomly targeted to autophagosomes and if the final outcome of autophagy is influenced by changes in mitochondrial morphology. Here we show that mitochondria unexpectedly elongate during macroautophagy. Mitochondrial elongation is triggered by PKA-mediated inhibition of DRP1 and is required to sustain cellular ATP levels and viability. Our results indicate that mitochondrial shape determines cellular fate during macroautophagy.

RESULTS

Mitochondria elongate on induction of autophagy

We assessed whether mitochondrial morphology is modified during autophagy. Confocal microscopy of wild-type mouse embryonic fibroblasts (MEFs) expressing a mitochondrially targeted yellow fluorescent protein (mtYFP) showed that induction of autophagy by starvation led to an early elongation of mitochondria resulting in a network of highly interconnected organelles (Fig. 1a,b). Elongation was observed as soon as 1 h after nutrient deprivation, was maintained for up to 48 h (data not shown) and occurred in all of the cell lines tested (mouse C2C12 myoblasts, human HeLa epithelial and HepG2 hepatocarcinoma cells), as well as in primary mouse hepatocytes (Supplementary Fig. S1a). Inactivation of the mammalian target of rapamycin (mTOR) metabolic sensor is another classical stimulus of autophagy. Efficient knockdown of mTOR mediated by short RNA interference also triggered mitochondrial elongation (Fig. 1c,d). Next, cells were co-transfected with mitochondrially targeted photoactivatable green fluorescent protein (mtPAGFP) and mitochondrially targeted red fluorescent protein (mtRFP). The dilution rate of mtPAGFP is proportional to productive fusion events[31]. The dilution rate increased on starvation in wild-type

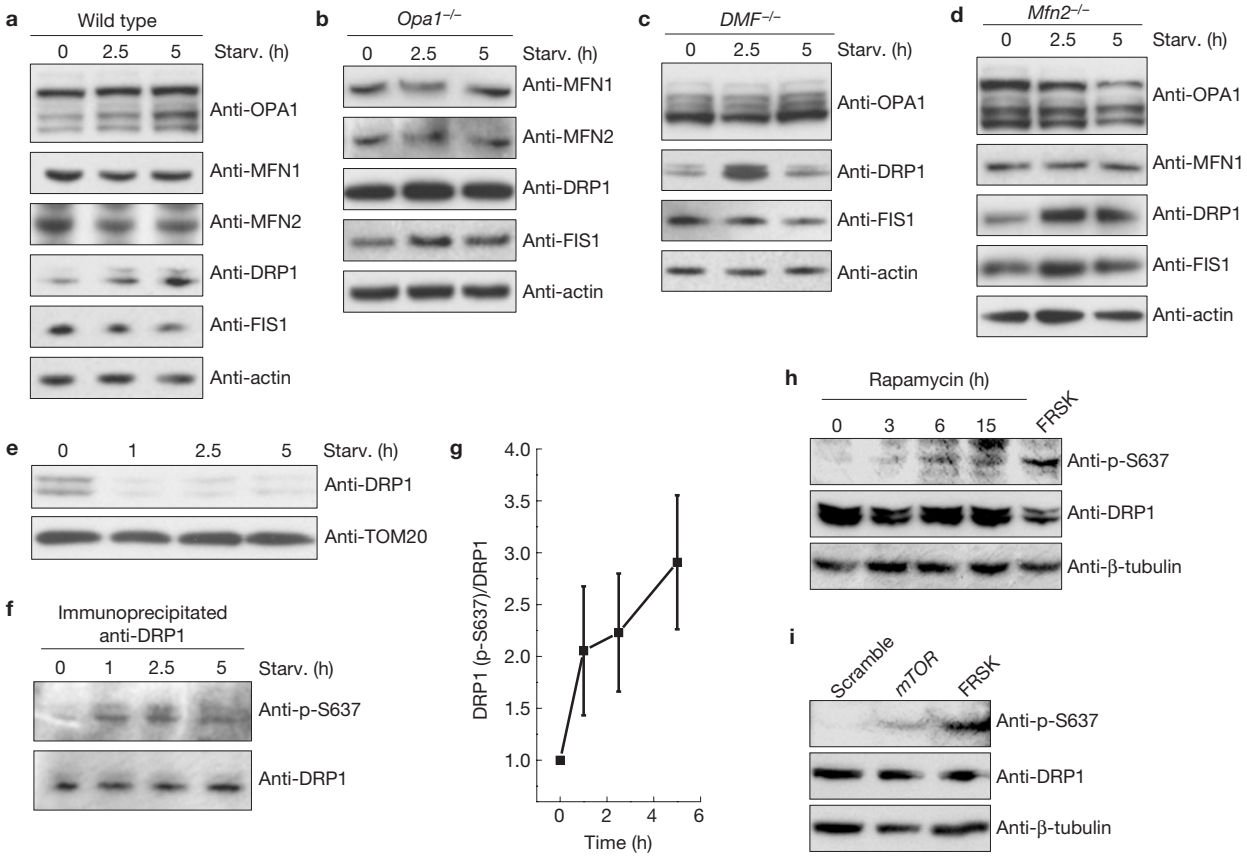

Figure 2 Increased phosphorylation of Ser 637 of DRP1 during autophagy. (**a**–**d**) Levels of mitochondria-shaping proteins during starvation. Protein samples (20 μg) from MEFs of the indicated genotype were separated by SDS–PAGE and immunoblotted with the indicated antibodies. Cells were starved for the indicated times. (**e**) Association of DRP1 with mitochondria during starvation. Mitochondria were isolated from MEFs starved for the indicated times and 25 μg samples of proteins were separated by SDS–PAGE and immunoblotted with the indicated antibodies. (**f**) Levels of Ser 637 phosphorylation of DRP1 during starvation. Equal amounts of cell lysates from wild-type MEFs starved for the indicated times were immunoprecipitated with the indicated antibody and the immunoprecipitated proteins were separated by SDS–PAGE and immunoblotted with the indicated antibodies. (**g**) Quantitative analysis of Ser 637 phosphorylation of DRP1 during starvation. Experiments were carried out as in **f**. Data are normalized to total levels of DRP1 and represent the mean ± s.e.m. of three independent experiments. (**h**) MEFs were treated for the indicated times with 100 nM rapamycin or with 25 μM forskolin (FRSK) for 0.5 h, lysed and equal amounts (50 μg) of proteins were separated by SDS–PAGE and immunoblotted using the indicated antibodies. (**i**) HeLa cells were transfected for 2 days with the indicated siRNA or treated with 25 μM forskolin for 0.5 h and lysed. Equal amounts (50 μg) of proteins were separated by SDS–PAGE and immunoblotted using the indicated antibodies. Uncropped images of all blots in this figure are shown in Supplementary Fig. S8.

as well as *Mfn2*$^{-/-}$ cells (Fig. 1e–g and Supplementary Movie S1). Accordingly, induction of autophagy led to mitochondrial elongation in *Mfn2*$^{-/-}$, but not in *Opa1*$^{-/-}$ (ref. 32) and *Mfn1*$^{-/-}$*Mfn2*$^{-/-}$ (*DMF*$^{-/-}$; ref. 33) MEFs, which lack the core components of the mitochondrial fusion machinery, and mitochondria remained elongated in *Drp1*$^{-/-}$ cells, in which fission is genetically impaired[34] (Fig. 1a,b). BAX (B-cell lymphoma 2 (BCL2)-associated X protein) and BAK (BCL2 antagonist killer 1) are necessary for fusion of mitochondria[18] and in their absence autophagy is enhanced as a default death mechanism[19]. In response to starvation, the *Bax*$^{-/-}$*Bak*$^{-/-}$ punctiform mitochondria also elongated (Supplementary Fig. S1c,d), indicating that BAX and BAK are not essential for elongation during induction of autophagy. In all of the MEFs tested, autophagic flux measured in the presence of bafilomycin A1 was comparable, as judged by processing of cytosolic light chain 3 (LC3-I) to the membrane bound form (LC3-II) and by degradation of p62 (Supplementary Fig. S2). In addition, mitochondrial elongation during starvation was still observed when proximal autophagic signalling was blocked by wortmannin (Supplementary Fig. S3) and in cells lacking the key component of the autophagic machinery, autophagy protein 5 (ATG5; data not shown). When autophagy was induced *in vivo* by fasting mice for 12 h, electron microscopy of muscle and liver revealed similar changes in mitochondrial morphology. Longitudinal sections of *tibialis anterior* from fasted mice showed that intermyofibrillar mitochondria were retrieved as one elongated organelle, no longer surrounded by glycogen granules; also in liver, perinuclear mitochondria were clearly elongated in fasted mice (Fig. 1h). In sum, mitochondrial elongation requires the core mitochondrial fusion machinery and is not dependent on autophagosome formation, which is conversely independent from mitochondrial elongation.

Mitochondrial elongation during autophagy depends on DRP1 phosphorylation by PKA

Mitochondrial hyperfusion can be triggered by a panoply of stress stimuli and depends on changes in OPA1 forms[20]. In response to

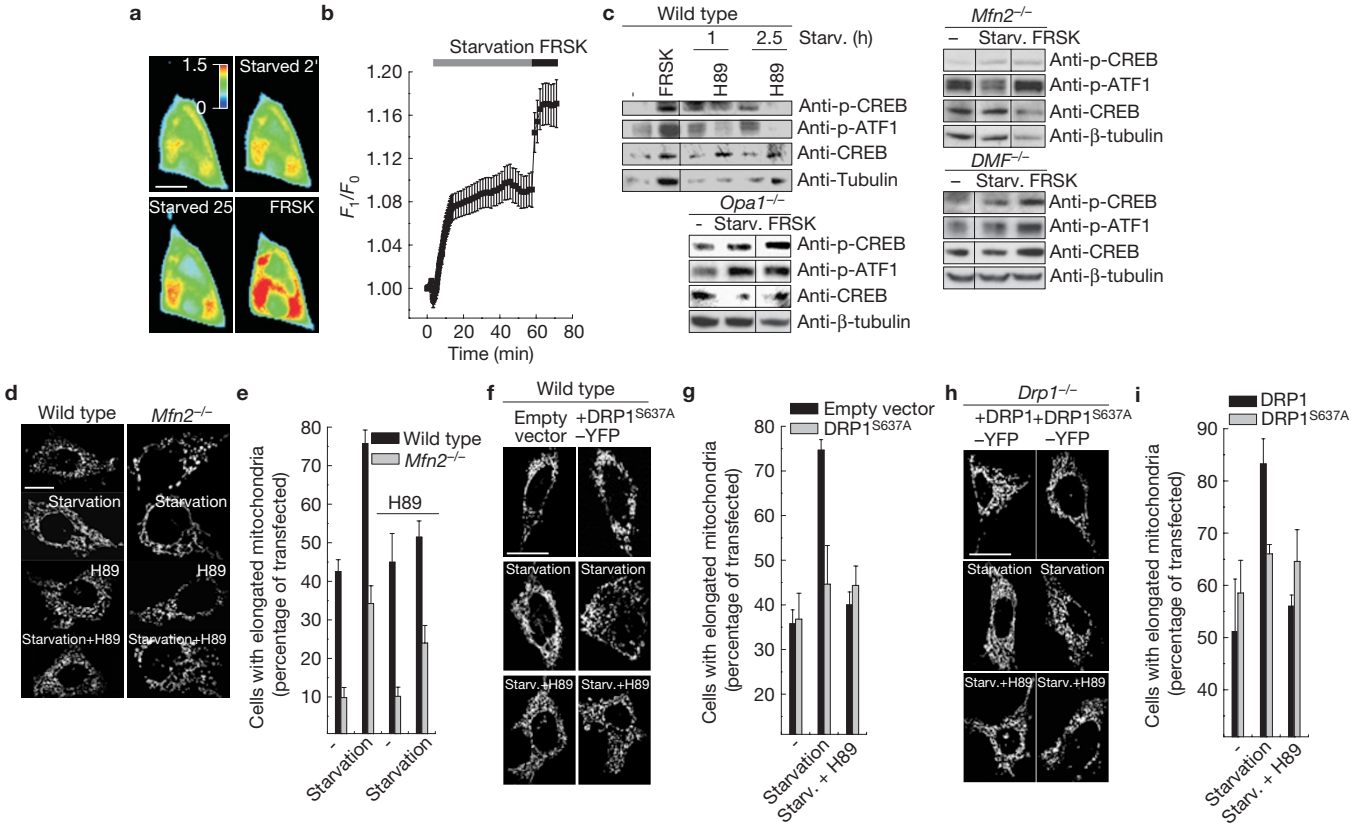

Figure 3 Mitochondrial elongation during starvation is mediated by the cAMP–PKA axis. (**a**) Pseudocolour-coded images of EPACI–camps FRET from real-time imaging of wild-type MEFs transfected with EPACI–camps. Where indicated, cells were perfused with the starvation solution for the indicated times (in min) or with 25 μM forskolin (FRSK). Scale bar, 20 μm. Colour scale indicates $F1/F0$ ratio. See also Supplementary Movie S3. (**b**) Quantitative analysis of CFP/YFP FRET ratio. Experiments were carried out as in **a**. Where indicated, cells were perfused with the starvation solution or with 25 μM forskolin. Data represent mean ± s.e.m. of 13 independent experiments. (**c**) Lysate samples (50 μg) from MEFs of the indicated genotypes were analysed by SDS–PAGE and immunoblotting using the indicated antibodies. Where indicated, MEFs were starved, or treated with 25 μM forskolin. Where indicated, 20 μM H89 was added during starvation. Uncropped images of all blots in this figure are shown in Supplementary Fig. S8. (**d**) Representative images of the effect of H89 on mitochondrial morphology on starvation. Wild-type and *Mfn2*$^{-/-}$ MEFs were transfected with mtYFP, and after 24 h confocal micrographs were acquired. Where indicated, cells were starved for 2.5 h and 20 μM H89 was added. Scale bar, 20 μm. (**e**) Morphometric analysis. Experiments were carried out as in **d**. Data represent mean ± s.e.m. of five independent experiments ($n = 100$ cells per condition). (**f**) Starvation-induced mitochondrial elongation depends on Ser 637 of DRP1. Representative confocal micrographs of mitochondrial morphology of wild-type MEFs co-transfected with mtRFP and the indicated plasmids. At 24 h after transfection, where indicated cells were starved for 2.5 h and imaged. Where indicated, 20 μM H89 was present during starvation. Scale bar, 20 μm. (**g**) Morphometric analysis of mitochondrial shape. Experiments were carried out as in **f**. Data represent mean ± s.e.m. of five independent experiments ($n = 50$ cells per condition). (**h**) Representative confocal micrographs of mitochondrial morphology of *Drp1*$^{-/-}$ MEFs co-transfected with mtRFP and the indicated plasmids. At 24 h after transfection, where indicated cells were starved for 2.5 h and imaged. Where indicated, 20 μM H89 was present during starvation. Scale bar, 20 μm. (**i**) Morphometric analysis of mitochondrial shape. Experiments were carried out as in **h**. Data represent mean ± s.e.m. of five independent experiments ($n = 50$ cells per condition).

starvation, however, levels of total as well as of individual forms of OPA1 were stable, similarly to those of MFN1, MFN2 and FIS1 (fission 1 homologue). The total amount of the fission protein DRP1 was slightly increased (Fig. 2a–d), but less DRP1 was associated with mitochondria during starvation (Fig. 2e). This result indicates that during starvation mitochondrial fusion is left unopposed. The kinase PKA and the phosphatase calcineurin regulate phosphorylation of the Ser 637 residue of DRP1, its translocation to mitochondria and therefore the intensity of mitochondrial fission[5]. Notably, during starvation the level of DRP1 Ser 637 phosphorylation was increased (Fig. 2f,g). Similarly, pharmacologic inhibition or silencing of mTOR resulted in an increased level of Ser 637 phosphorylation (Fig. 2h,i). Increased levels of phosphorylation could result from PKA activation or calcineurin inhibition: we therefore examined levels of the proximal PKA activator cAMP in response to starvation using a genetically encoded EPAC (exchange protein directly activated by cAMP)-based fluorescence resonance energy transfer (FRET) probe (EPACI–camps). Real-time imaging showed that there was a robust increase in cAMP levels when MEFs were switched from a nutrient-rich to 'starvation' medium (Fig. 3a,b). This increase resulted in the downstream activation of PKA, as measured by the phosphorylation of the PKA targets CREB (cAMP-response element-binding protein) and ATF1 (activating transcription factor 1). Phosphorylation of CREB and AFT1 was sensitive to H89, a pharmacological inhibitor of PKA (Fig. 3c). Activation of PKA was detected in all of the other cell lines (mouse C2C12, human HeLa and HepG2), in which starvation induced mitochondrial elongation (Supplementary Fig. S1b). PKA activation was comparable in cells in which mitochondria did (wild-type and

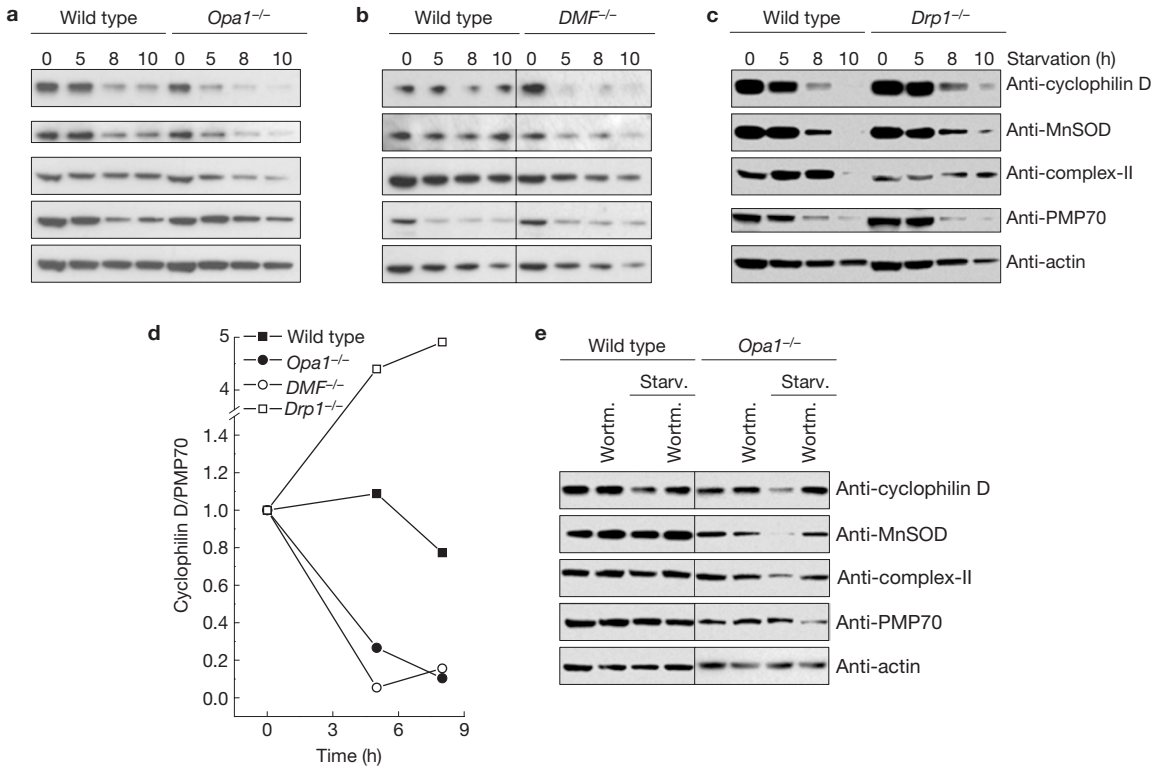

Figure 4 Elongated mitochondria are spared from degradation during starvation. (**a**–**c**) MEFs of the indicated genotype were treated as indicated, counted and 2.7×10^5 cells were lysed. Lysates were separated by SDS–PAGE and immunoblotted using the indicated antibodies. (**d**) Ratio between the densitometric levels of cyclophilin D and those of PMP70 in MEFs of the indicated genotype. One representative experiment of five independent repetitions performed as in **a**–**c** is shown. (**e**) MEFs of the indicated genotype starved for 5 h were treated where indicated with 0.5 μM wortmannin (Wortm.). Lysates from 2.7×10^5 cells were separated by SDS–PAGE and immunoblotted with the indicated antibodies. Uncropped images of all blots in this figure are shown in Supplementary Fig. S8.

Mfn2$^{-/-}$) and did not (*Opa1*$^{-/-}$ and *DMF*$^{-/-}$) elongate in response to starvation (Fig. 3c), indicating that activation does not depend on mitochondrial morphology. The PKA inhibitor H89 blocked mitochondrial elongation during starvation (Fig. 3d,e), indicating that PKA activation is an essential step for mitochondrial elongation. Consistently, an increase in cAMP levels obtained pharmacologically led to mitochondrial elongation (Supplementary Fig. S4). To test whether the activation of PKA impinged on DRP1, we used a genetic approach. In MEFs expressing a DRP1–YFP chimaera mutated in the PKA phosphorylation site (DRP1^{S637A}–YFP; ref. 5), mitochondria were unable to elongate during starvation, and inhibition of PKA had no effect on morphology (Fig. 3f,g). Finally, we reconstituted *Drp1*$^{-/-}$ MEFs with levels of DRP1–YFP or DRP1^{S637A}–YFP comparable to those of endogenous DRP1. In the reconstituted cells, mitochondria reverted to short rods and starvation could induce H89-sensitive elongation only when MEFs were complemented with DRP1–YFP, but not with DRP1^{S637A}–YFP (Fig. 3h,i). Thus, during starvation, the activation of PKA impinges on DRP1 to trigger mitochondrial elongation.

Elongated mitochondria are spared from autophagic degradation and maintain ATP levels during starvation

Fragmentation of dysfunctional mitochondria precedes mitophagy, indicative of a role for mitochondrial elongation during autophagy in maintenance of the mitochondrial mass. Following starvation, mitochondrial proteins (cyclophilin D, manganese superoxide dismutase (MnSOD) and a subunit of complex-II) were lost more rapidly in *Opa1*$^{-/-}$ (Fig. 4a) and *DMF*$^{-/-}$ (Fig. 4b) cells that did not elongate mitochondria, but were retained in *Drp1*$^{-/-}$ cells (Fig. 4c,d). These quantitative immunoblotting data were confirmed by confocal microscopy analysis of co-localization[30] of mitochondria with YFP–LC3-labelled autophagosomes (Supplementary Fig. S5). No differences were observed in the rate of degradation of proteins from other subcellular compartments (the peroxisomal membrane protein PMP70, which has a relative molecular mass of 70,000, and the cytosolic protein actin). Furthermore, wortmannin, which blocks autophagosome formation, prevented mitochondrial elimination, indicating that mitochondria were degraded by autophagy (Fig. 4e). Increased degradation could be supported by dysfunction of *Opa1*$^{-/-}$ mitochondria during starvation. Although during starvation the accumulation of the potentiometric fluorescent dye tetramethyl rhodamine methylester (TMRM) was higher in *Opa1*$^{-/-}$ cells (Supplementary Fig. S6a), an assay for latent mitochondrial dysfunction revealed that mitochondria of starved *Opa1*$^{-/-}$ MEFs maintain their membrane potential by using the reversal of the ATPase (ref. 21; Fig. 5a,b). Accordingly, total cellular ATP levels decreased in *Opa1*$^{-/-}$ and *DMF*$^{-/-}$ cells during starvation (Fig. 5c). Reduced mitochondrial ATP production contributed to these decreased total cellular ATP levels, whereas wild-type organelles in which elongation occurs were able to sustain ATP output, as indicated by monitoring mitochondrial ATP levels *in situ* using a genetically encoded luciferase probe targeted to the matrix of the organelle[35] (Fig. 5d). The free energy of the electrochemical potential is used by the mitochondrial

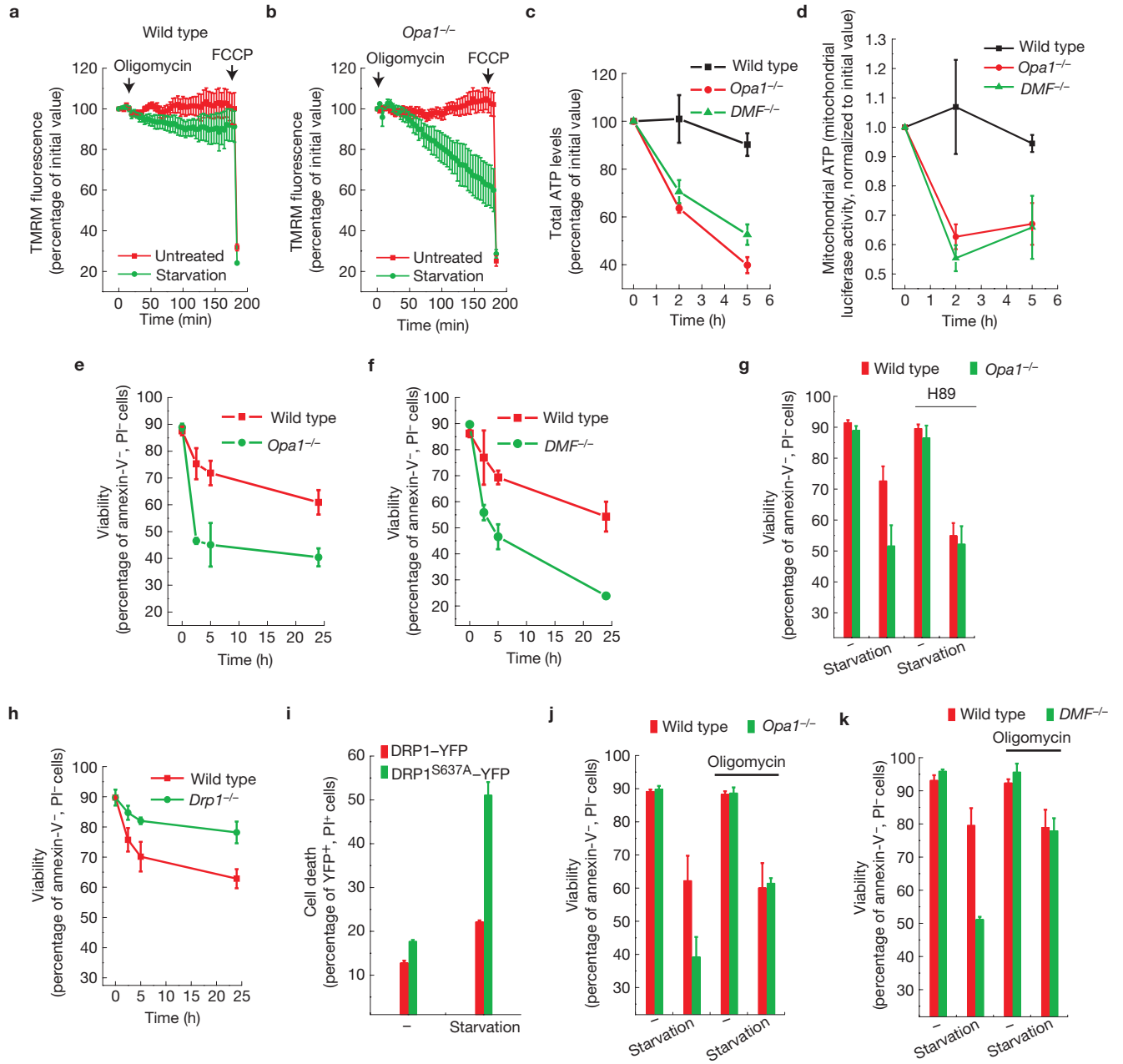

Figure 5 Mitochondrial elongation sustains cellular ATP production and viability during autophagy. (**a**,**b**) Quantitative analysis of TMRM fluorescence changes over mitochondrial regions in MEFs of the indicated genotype. Where indicated, cells were starved for 5 h before TMRM loading. Where indicated (arrows), 2.5 μg ml^{-1} oligomycin and 2 μM carbonyl cyanide-p-trifluoromethoxyphenylhydrazone (FCCP) were added. Data represent mean ± s.e.m. of seven independent experiments. (**c**) Total cellular ATP levels were measured in cells of the indicated genotype starved for the indicated times. Data represent mean ± s.e.m. of five independent experiments. (**d**) Mitochondrial ATP measured *in situ* by mitochondrially targeted luciferase in cells of the indicated genotype starved for the indicated times. Data represent mean ± s.e.m. of five independent experiments and are normalized to the initial value. (**e**,**f**) Cells of the indicated genotype were starved for the indicated times. Viability was determined by flow cytometry as the percentage of annexin-V- and propidium iodide (PI)-negative events. Data represent mean ± s.e.m. of five independent experiments. (**g**) MEFs of the indicated genotype were starved for 2.5 h. Where indicated, cells were treated with 20 μM H89. Viability was determined as in **e**,**f**. Data represent mean ± s.e.m. of five independent experiments. (**h**) Cells of the indicated genotype were starved for the indicated times. Viability was determined as in **e**,**f**. Data represent mean ± s.e.m. of five independent experiments. (**i**) *Drp1*$^{-/-}$ MEFs were transfected with the indicated plasmids and after 24 h starved for 5 h where indicated. Cell death was determined by flow cytometry as the percentage of YFP- and propidium-iodide-positive events. Data represent mean ± s.e.m. of four independent experiments. (**j**,**k**) MEFs of the indicated genotype were starved for 5 h in the presence of 2.5 μg ml^{-1} oligomycin where indicated. Viability was determined as in **e**,**f**. Data represent mean ± s.e.m. of five independent experiments.

ATPase to synthesize ATP (ref. 36). Although isolated ATPase is fully active as a monomer, the enzyme is ubiquitously found in more-efficient dimeric and oligomeric forms[37]. Blue-native gel electrophoresis on whole cells enabled investigation of the ATP synthase organization and activity during starvation without isolating mitochondria (and therefore disrupting their morphology). The

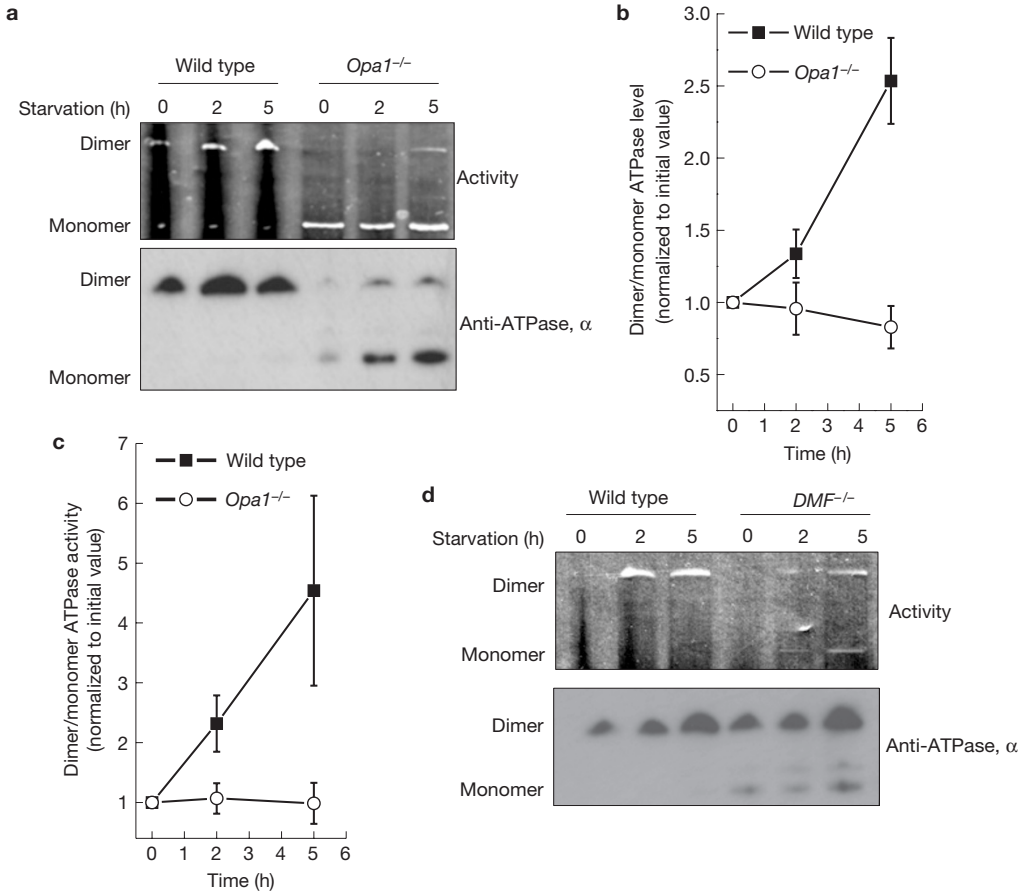

Figure 6 Mitochondrial elongation during starvation is associated with dimerization and activation of ATPase. (**a**) Blue-native electrophoresis analysis of ATPase dimerization and activity. Cells of the indicated genotype were treated as indicated and 500 μg of total cell extract was solubilized with 4% digitonin and proteins were separated by blue-native PAGE. ATPase activity was measured in-gel (top) and ATPase levels were measured by immunoblotting for the indicated antibody (bottom). (**b**,**c**) Quantitative analysis of the ratio of levels (**b**) and activity (**c**) between dimeric and monomeric forms of ATPase, assessed by densitometric analysis of gels from experiments performed as in **a**. Data represent mean ± s.e.m. of five independent experiments. (**d**) Experiments were carried out as in **a**, but with cells of the indicated genotype.

total levels of ATP synthase increased on starvation as indicated by specific immunoblotting (Supplementary Fig. S6b). In wild-type, but not *Opa1*$^{-/-}$ or *DMF*$^{-/-}$, MEFs the ratio between the dimeric and the monomeric form of the ATPase was higher already in non-starved cells and increased during starvation, as demonstrated by a specific in-gel activity assay for ATPase activity (Fig. 6). Dimerization of ATPase correlates with formation of cristae[37,38]. However, the opposite can also be true, that increased cristae surface area favours oligomerization of the ATPase. Electron microscopy and morphometric analysis showed that the number of cristae per unit of mitochondrial surface increased during starvation in wild-type and *Mfn2*$^{-/-}$ mitochondria that elongate, whereas it remained stable in *Opa1*$^{-/-}$ and *DMF*$^{-/-}$ mitochondria that do not (Fig. 7a–c). Thus, during starvation mitochondrial elongation correlates with increased cristae surface area, oligomerization of the ATPase and maintenance of mitochondrial ATP production.

Mitochondrial elongation protects cells from death during starvation

Next, we addressed the role of starvation-induced elongation in the cellular response to nutrient depletion. *Opa1*$^{-/-}$ and *DMF*$^{-/-}$ as well as cells in which PKA was inhibited (Fig. 5e–g) died more rapidly, whereas *Drp1*$^{-/-}$ MEFs were less susceptible to starvation (Fig. 5h). The increased level of death by starvation of cells treated with H89 was phenocopied in *Drp1*$^{-/-}$ MEFs reconstituted with the DRP1^{S637A} mutant (Fig. 5i). Knockdown of *OPA1* in HeLa cells also accelerated starvation-induced cell death (Supplementary Fig. S7a,b). Death of *Opa1*$^{-/-}$ and *DMF*$^{-/-}$ MEFs was prevented by the ATPase inhibitor oligomycin (Fig. 5j,k), in accordance with the fact that mitochondria unable to elongate during starvation maintain their membrane potential by hydrolysing and consuming cellular ATP (Fig. 5b,c). In conclusion, mitochondria unable to elongate during nutrient deprivation consume cellular ATP, leading to cell death.

DISCUSSION

We have demonstrated that during starvation mitochondria elongate and that this is a critical component of the cellular response to autophagy. In starving cells, a rapid increase in cAMP levels activates PKA, which in turn phosphorylates DRP1, keeping it in the cytosol and allowing unopposed mitochondrial fusion. Elongated mitochondria are protected from autophagic elimination and have a higher density of cristae, which favours oligomerization of ATPase to maintain ATP production and to allow survival of starving cells. On the contrary, if elongation is blocked, mitochondria become dysfunctional and

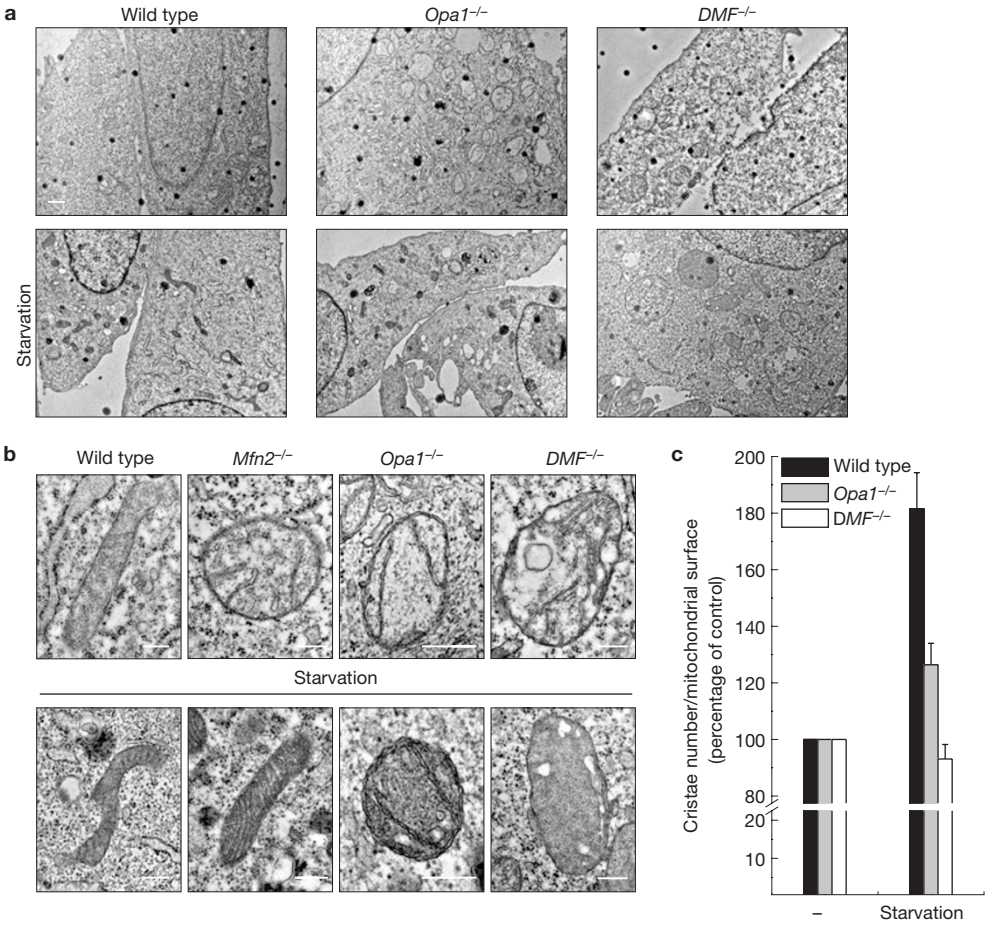

Figure 7 Density of cristae increases in mitochondria elongated during starvation. (**a**) Representative electron micrographs of cells of the indicated genotype starved where indicated for 5 h, fixed and processed for electron microscopy. Scale bar, 2 μm. (**b**) Representative electron micrographs of randomly selected mitochondria from cells of the indicated genotype. Where indicated, cells were starved for 5 h. Scale bars, 0.5 μm. (**c**) Morphometric analysis of cristae density in cells of the indicated genotype. Experiments were carried out as in **a**. The number of cristae in 50 randomly selected mitochondria of the indicated genotype was normalized for the calculated surface of the organelle. Data represent mean ± s.e.m. of five independent experiments.

'cannibalize' cytoplasmic ATP to maintain their membrane potential, precipitating cell death (Fig. 8).

Macroautophagy triggered by nutrient deprivation degrades different constituents of the cell to allow their recycling. If mitochondria were also to be targeted to the autophagosome, their fragmentation should precede engulfment, as it occurs during selective mitochondrial autophagy[18]. However, in response to stimuli that induce macroautophagy, mitochondria elongate as a consequence of DRP1 phosphorylation at Ser 637 by PKA, triggered by an increase in cAMP levels. Interestingly, glucagon, the prototypical inducer of autophagy in liver, induces cAMP elevation in hepatocytes[39]. Here we extend the importance of cAMP in starvation-induced autophagy in tissues other than liver. In yeast, activation of PKA is important in pseudohyphal differentiation triggered by nitrogen starvation[40]. Conversely, constitutive activation of PKA inhibits autophagosome formation[41,42], indicating that the PKA loop clarified here may be specific for multicellular eukaryotes. The yeast orthologue of DRP1 lacks a conserved PKA phosphorylation site, indicating that the metabolic response of yeast mitochondria during autophagy is differentially regulated. Elongation and phosphorylation of DRP1 occurs also in response to inactivation of the metabolic sensor mTOR, indicative of an interplay with PKA that is supported in different paradigms in mammals[43] and in yeast[44]. Several mechanisms are responsible for the changes in mitochondrial shape triggered by external and internal cues. For example, in cells exposed to several stresses, a change in the relative levels of the forms of the pro-fusion OPA1 supports mitochondrial elongation[45], whereas during apoptosis mitochondrial fragmentation is supported by the inhibition of mitochondrial fusion[46] through the stimulation of DRP1 translocation to mitochondria[47], where it is stabilized by BAX- and BAK-dependent SUMOylation[48]. Conversely, during starvation, the forms of OPA1 remain stable, but mitochondrial levels of DRP1 are reduced. Multiple pieces of biochemical and genetic evidence support the finding that the reduced levels of mitochondrial DRP1 are a consequence of its phosphorylation by activated PKA. Alternatively, another interesting possibility could be that during macroautophagy mitochondrial DRP1 is not stabilized by SUMOylation, being then ubiquitylated by resident mitochondrial ubiquitin ligases[49,50], and degraded in a proteasome-dependent fashion. In agreement, following induction of mitophagy the ubiquitin ligase Parkin degrades components of the mitochondrial fusion machinery[51,52] and targets dysfunctional organelles to the autophagosome[53]. However, starvation-

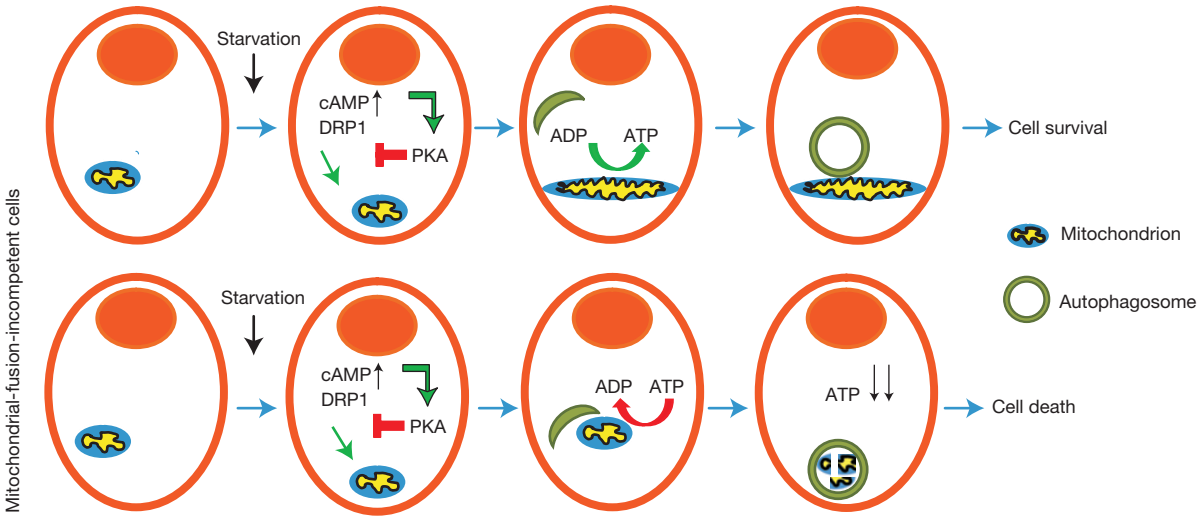

Figure 8 Mitochondrial elongation induced by PKA determines cell fate during starvation. The diagrams depict the cascade of mitochondrial elongation triggered during starvation and its role in determining cell fate. Top row: mitochondrial elongation protects it from organelle degradation and allows maintenance of ATP levels. Bottom row: when mitochondrial elongation is impaired, mitochondria are degraded and the remaining organelles consume cellular ATP, precipitating cell death.

induced mitochondrial elongation occurs also in HeLa cells in which Parkin is not expressed[53], further substantiating the key role of the cAMP–PKA–DRP1 loop in autophagy. Opposed to the 'active' adaptation of mitochondrial morphology in response to the cellular cues described here, lies the pathological DRP1-mediated fragmentation by sustained activation of calcineurin, such as that observed in Huntington's disease, which results in increased susceptibility to apoptotic insults[54]. These two extremes show how mitochondrial morphology is extremely sensitive to, and plastically modulated by, cellular inputs.

The purpose of mitochondrial elongation during induction of autophagy remains unclear. Elongated mitochondria are spared from autophagy, implying that the 'targets' for degradation during macroautophagy may not be random. The limitation could be simply sterical—that is, the elongated mitochondria cannot fit into the autophagosome. Alternatively, longer mitochondria may lack the signal that addresses them to the autophagosome. In this respect, it is interesting to note that shorter mitochondria are not only less efficient in ATP production, but they also bear a latent dysfunction that could trigger the relocalization of Parkin on their surface[53]. Mitochondria may be spared by macroautophagy because during nutrient restriction, cells try to maximize the efficiency of energy conversion, a task for which mitochondria are optimized[55] and that requires mitochondrial elongation, as we showed here. Elongated mitochondria have higher levels of the dimeric form of ATPase, associated with increased efficiency in ATP production[37]. Morphologically, this is mirrored by an increase in the number of cristae, the privileged compartments for ATP synthesis[37], per unit of mitochondrial surface. Whereas OPA1 and cristae organization are directly linked[56,57], it is less clear why $DMF^{-/-}$MEFs are unable to respond to starvation with an increase in cristae biogenesis. However, OPA1 forms are altered in $DMF^{-/-}$MEFs and knockdown of DRP1 similarly alters processing of OPA1 (ref. 58). Thus, it seems that processing of OPA1 (and hence biogenesis of the cristae) is exquisitely sensitive to changes in the fusion–fission equilibrium, ultimately impacting on the ability of the mitochondria to metabolically respond to the environment. In addition, mitochondria may be essential to provide membranes for the formation of the autophagosome[29] and they should therefore be excluded from immediate degradation, to ensure the progression of the autophagic process.

During starvation, mitochondria unable to elongate are latently dysfunctional and they consume cytosolic ATP to sustain their membrane potential. The ensuing bioenergetic crisis due to ATP consumption causes starvation-induced cell death in $Opa1^{-/-}$ and $DMF^{-/-}$MEFs. As expected, during starvation autophagy is essential to provide nutrients and its blockage accelerates death[59], irrespective of whether mitochondrial elongation occurs or not. Whether the protective role of autophagy is a general feature of all forms of cell death remains a matter of intense debate. Our data conversely indicate that changes in mitochondrial morphology and function are an essential subroutine of the autophagic programme: if a stereotypical response of the cell (mitochondrial elongation and activation) to limited nutrient supply is abolished, the ensuing mitochondrial dysfunction can lead to cell death. The unexpected role of mitochondrial elongation during starvation exemplifies a further cellular response regulated by these organelles. □

METHODS

Methods and any associated references are available in the online version of the paper at http://www.nature.com/naturecellbiology/

Note: Supplementary Information is available on the Nature Cell Biology website

ACKNOWLEDGEMENTS

L.C.G. is the recipient of a 'Bolsa de Doutoramento' of the 'Fundação para a Ciência e Tecnologia', Portugal. L.S. is a Senior Telethon Scientist of the Dulbecco-Telethon Institute. This research was supported by Telethon Italy S02016, AIRC Italy, Swiss National Foundation SNF 31-118171. We thank D. Chan, K. Mihara, C. Blackstone and N. Mizushima for reagents and T. Pozzan for helpful discussions on mitochondrially targeted luciferase calibration.

AUTHOR CONTRIBUTIONS

L.C.G. and L.S. conceived research, analysed data and wrote the manuscript. L.C.G., G.D.B. and L.S. carried out experiments and analysed data.

COMPETING FINANCIAL INTERESTS

The authors declare no competing financial interests.

Published online at http://www.nature.com/naturecellbiology
Reprints and permissions information is available online at http://npg.nature.com/reprintsandpermissions/

1. Bereiter-Hahn, J. & Voth, M. Dynamics of mitochondria in living cells: shape changes, dislocations, fusion, and fission of mitochondria. *Microsc. Res. Tech.* **27,** 198–219 (1994).
2. Cipolat, S., de Brito, O. M., Dal Zilio, B. & Scorrano, L. OPA1 requires mitofusin 1 to promote mitochondrial fusion. *Proc. Natl Acad. Sci. USA* **101,** 15927–15932 (2004).
3. Santel, A. & Fuller, M. T. Control of mitochondrial morphology by a human mitofusin. *J. Cell Sci.* **114,** 867–874 (2001).
4. Smirnova, E., Griparic, L., Shurland, D. L. & van der Bliek, A. M. Dynamin-related protein Drp1 is required for mitochondrial division in mammalian cells. *Mol. Biol. Cell* **12,** 2245–2256 (2001).
5. Cereghetti, G. M. *et al.* Dephosphorylation by calcineurin regulates translocation of Drp1 to mitochondria. *Proc. Natl Acad. Sci. USA* **105,** 15803–15808 (2008).
6. Cribbs, J. T. & Strack, S. Reversible phosphorylation of Drp1 by cyclic AMP-dependent protein kinase and calcineurin regulates mitochondrial fission and cell death. *EMBO Rep.* **8,** 939–944 (2007).
7. Chang, C. R. & Blackstone, C. Cyclic AMP-dependent protein kinase phosphorylation of Drp1 regulates its GTPase activity and mitochondrial morphology. *J. Biol. Chem.* **282,** 21583–21587 (2007).
8. Harder, Z., Zunino, R. & McBride, H. Sumo1 conjugates mitochondrial substrates and participates in mitochondrial fission. *Curr. Biol.* **14,** 340–345 (2004).
9. Braschi, E., Zunino, R. & McBride, H. M. MAPL is a new mitochondrial SUMO E3 ligase that regulates mitochondrial fission. *EMBO Rep.* **10,** 748–754 (2009).
10. Scorrano, L. *et al.* A distinct pathway remodels mitochondrial cristae and mobilizes cytochrome *c* during apoptosis. *Dev. Cell* **2,** 55–67 (2002).
11. Martinou, I. *et al.* The release of cytochrome c from mitochondria during apoptosis of NGF-deprived sympathetic neurons is a reversible event. *J. Cell Biol.* **144,** 883–889 (1999).
12. Frank, S. *et al.* The role of dynamin-related protein 1, a mediator of mitochondrial fission, in apoptosis. *Dev. Cell* **1,** 515–525 (2001).
13. Szabadkai, G. *et al.* Drp-1-dependent division of the mitochondrial network blocks intraorganellar Ca^{2+} waves and protects against Ca^{2+}-mediated apoptosis. *Mol. Cell* **16,** 59–68 (2004).
14. Li, Z., Okamoto, K., Hayashi, Y. & Sheng, M. The importance of dendritic mitochondria in the morphogenesis and plasticity of spines and synapses. *Cell* **119,** 873–887 (2004).
15. Campello, S. *et al.* Orchestration of lymphocyte chemotaxis by mitochondrial dynamics. *J. Exp. Med.* **203,** 2879–2886 (2006).
16. Mitra, K., Wunder, C., Roysam, B., Lin, G. & Lippincott-Schwartz, J. A hyperfused mitochondrial state achieved at G1-S regulates cyclin E buildup and entry into S phase. *Proc. Natl Acad. Sci. USA* **106,** 11960–11965 (2009).
17. Scheckhuber, C. Q. *et al.* Reducing mitochondrial fission results in increased life span and fitness of two fungal ageing models. *Nat. Cell Biol.* **9,** 99–105 (2007).
18. Twig, G. *et al.* Fission and selective fusion govern mitochondrial segregation and elimination by autophagy. *EMBO J.* **27,** 433–446 (2008).
19. Gomes, L. C. & Scorrano, L. High levels of Fis1, a pro-fission mitochondrial protein, trigger autophagy. *Biochim. Biophys. Acta* **1777,** 860–866 (2008).
20. Klionsky, D. J. & Emr, S. D. Autophagy as a regulated pathway of cellular degradation. *Science* **290,** 1717–1721 (2000).
21. Cecconi, F. & Levine, B. The role of autophagy in mammalian development: cell makeover rather than cell death. *Dev. Cell* **15,** 344–357 (2008).
22. Ravikumar, B., Duden, R. & Rubinsztein, D. C. Aggregate-prone proteins with polyglutamine and polyalanine expansions are degraded by autophagy. *Hum. Mol. Genet.* **11,** 1107–1117 (2002).
23. Zheng, Y. T. *et al.* The adaptor protein p62/SQSTM1 targets invading bacteria to the autophagy pathway. *J. Immunol.* **183,** 5909–5916 (2009).
24. Tuttle, D. L., Lewin, A. S. & Dunn, W. A. Jr Selective autophagy of peroxisomes in methylotrophic yeasts. *Eur. J. Cell Biol.* **60,** 283–290 (1993).
25. Bernales, S., McDonald, K. L. & Walter, P. Autophagy counterbalances endoplasmic reticulum expansion during the unfolded protein response. *PLoS Biol.* **4,** e423 (2006).
26. Elmore, S. P., Qian, T., Grissom, S. F. & Lemasters, J. J. The mitochondrial permeability transition initiates autophagy in rat hepatocytes. *FASEB J.* **15,** 2286–2287 (2001).
27. Tooze, S. A. & Yoshimori, T. The origin of the autophagosomal membrane. *Nat. Cell Biol.* **12,** 831–835 (2010).
28. Scherz-Shouval, R. *et al.* Reactive oxygen species are essential for autophagy and specifically regulate the activity of Atg4. *EMBO J.* **26,** 1749–1760 (2007).
29. Hailey, D. W. *et al.* Mitochondria supply membranes for autophagosome biogenesis during starvation. *Cell* **141,** 656–667 (2010).
30. de Brito, O. M. & Scorrano, L. Mitofusin 2 tethers endoplasmic reticulum to mitochondria. *Nature* **456,** 605–610 (2008).
31. Karbowski, M. *et al.* Quantitation of mitochondrial dynamics by photolabelling of individual organelles shows that mitochondrial fusion is blocked during the Bax activation phase of apoptosis. *J. Cell Biol.* **164,** 493–499 (2004).
32. Song, Z., Chen, H., Fiket, M., Alexander, C. & Chan, D. C. OPA1 processing controls mitochondrial fusion and is regulated by mRNA splicing, membrane potential, and Yme1L. *J. Cell Biol.* **178,** 749–755 (2007).
33. Chen, H., Chomyn, A. & Chan, D. C. Disruption of fusion results in mitochondrial heterogeneity and dysfunction. *J. Biol. Chem.* **280,** 26185–26192 (2005).
34. Ishihara, N. *et al.* Mitochondrial fission factor Drp1 is essential for embryonic development and synapse formation in mice. *Nat. Cell Biol.* **11,** 958–966 (2009).
35. Jouaville, L. S., Pinton, P., Bastianutto, C., Rutter, G. A. & Rizzuto, R. Regulation of mitochondrial ATP synthesis by calcium: evidence for a long-term metabolic priming. *Proc. Natl Acad. Sci. USA* **96,** 13807–13812 (1999).
36. Rich, P. Chemiosmotic coupling: the cost of living. *Nature* **421,** 583 (2003).
37. Strauss, M., Hofhaus, G., Schroder, R. R. & Kuhlbrandt, W. Dimer ribbons of ATP synthase shape the inner mitochondrial membrane. *EMBO J.* **27,** 1154–1160 (2008).
38. Giraud, M. F. *et al.* Is there a relationship between the supramolecular organization of the mitochondrial ATP synthase and the formation of cristae? *Biochim. Biophys. Acta* **1555,** 174–180 (2002).
39. Unger, R. H. Glucagon physiology and pathophysiology in the light of new advances. *Diabetologia* **28,** 574–578 (1985).
40. Pan, X. & Heitman, J. Cyclic AMP-dependent protein kinase regulates pseudohyphal differentiation in *Saccharomyces cerevisiae*. *Mol. Cell Biol.* **19,** 4874–4887 (1999).
41. Budovskaya, Y. V., Stephan, J. S., Reggiori, F., Klionsky, D. J. & Herman, P. K. The Ras/cAMP-dependent protein kinase signalling pathway regulates an early step of the autophagy process in *Saccharomyces cerevisiae*. *J. Biol. Chem.* **279,** 20663–20671 (2004).
42. Stephan, J. S., Yeh, Y. Y., Ramachandran, V., Deminoff, S. J. & Herman, P. K. The Tor and PKA signalling pathways independently target the Atg1/Atg13 protein kinase complex to control autophagy. *Proc. Natl Acad. Sci.* **106,** 17049–17054 (2009).
43. Mavrakis, M., Lippincott-Schwartz, J., Stratakis, C. A. & Bossis, I. Depletion of type IA regulatory subunit (RIalpha) of protein kinase A (PKA) in mammalian cells and tissues activates mTOR and causes autophagic deficiency. *Hum. Mol. Genet.* **15,** 2962–2971 (2006).
44. Slattery, M. G., Liko, D. & Heideman, W. Protein kinase A, TOR, and glucose transport control the response to nutrient repletion in *Saccharomyces cerevisiae*. *Eukaryot. Cell* **7,** 358–367 (2008).
45. Tondera, D. *et al.* SLP-2 is required for stress-induced mitochondrial hyperfusion. *EMBO J.* **28,** 1589–1600 (2009).
46. Karbowski, M. & Youle, R. J. Dynamics of mitochondrial morphology in healthy cells and during apoptosis. *Cell Death Differ.* **10,** 870–880 (2003).
47. Cereghetti, G. M., Costa, V. & Scorrano, L. Inhibition of Drp1-dependent mitochondrial fragmentation and apoptosis by a polypeptide antagonist of calcineurin. *Cell Death Differ.* **17,** 1785–1794 (2010).
48. Wasiak, S., Zunino, R. & McBride, H. M. Bax/Bak promote sumoylation of DRP1 and its stable association with mitochondria during apoptotic cell death. *J. Cell Biol.* **177,** 439–450 (2007).
49. Nakamura, N., Kimura, Y., Tokuda, M., Honda, S. & Hirose, S. MARCH-V is a novel mitofusin 2- and Drp1-binding protein able to change mitochondrial morphology. *EMBO Rep.* **7,** 1019–1022 (2006).
50. Karbowski, M., Neutzner, A. & Youle, R. J. The mitochondrial E3 ubiquitin ligase MARCH5 is required for Drp1 dependent mitochondrial division. *J. Cell Biol.* **178,** 71–84 (2007).
51. Tanaka, A. *et al.* Proteasome and p97 mediate mitophagy and degradation of mitofusins induced by Parkin. *J. Cell Biol.* **191,** 1367–1380 (2010).
52. Ziviani, E., Tao, R. N. & Whitworth, A. J. *Drosophila* parkin requires PINK1 for mitochondrial translocation and ubiquitinates mitofusin. *Proc. Natl Acad. Sci. USA* **107,** 5018–5023 (2010).
53. Narendra, D., Tanaka, A., Suen, D. F. & Youle, R. J. Parkin is recruited selectively to impaired mitochondria and promotes their autophagy. *J. Cell Biol.* **183,** 795–803 (2008).
54. Costa, V. *et al.* Mitochondrial fission and cristae disruption increase the response of cell models of Huntington's disease to apoptotic stimuli. *EMBO Mol. Med.* **2,** 490–503 (2010).
55. Brown, G. C. Control of respiration and ATP synthesis in mammalian mitochondria and cells. *Biochem. J.* **284,** 1–13 (1992).
56. Frezza, C. *et al.* OPA1 controls apoptotic cristae remodeling independently from mitochondrial fusion. *Cell* **126,** 177–189 (2006).
57. Meeusen, S. *et al.* Mitochondrial inner-membrane fusion and crista maintenance requires the dynamin-related GTPase Mgm1. *Cell* **127,** 383–395 (2006).
58. Mopert, K. *et al.* Loss of Drp1 function alters OPA1 processing and changes mitochondrial membrane organization. *Exp. Cell Res.* **315,** 2165–2180 (2009).
59. Kuma, A. *et al.* The role of autophagy during the early neonatal starvation period. *Nature* **432,** 1032–1036 (2004).

METHODS

Molecular biology. pEYFP-Mito (mtYFP), mito-dsRED (mtRFP), DRP1–YFP and DRP1^{S637A}–YFP were described previously[5]. mtPAGFP (ref. 46) was from M. Karbowski (University of Maryland, USA). EPACI–camps[60] was from M. Lohse (University of Würzburg, Germany). Mitochondrially targeted luciferase[35] was from R. Rizzuto (University of Padova, Italy).

Two short interfering RNAs (siRNAs) against the following target sequences from mouse *mTOR* were synthesized: 5′-GCGGAUGGCUCCUGACUAU-3′ and 5′-CCAAGGUGCUACAGUACUA-3′. An siRNA against the following target sequence from human *mTOR* was synthesized: 5′-UAACAGGUUCGAGAUAAG-3′. The scrambled control was used at the same final concentration (Dharmacon). The siRNA against human *OPA1* targeted the 5′-GGACCUUAGUGAAUAUAAA-3′ sequence (Ambion).

Cell culture. Simian virus 40 (SV40)-transformed wild-type, *Mfn1*$^{-/-}$, *Mfn2*$^{-/-}$ and *DMF*$^{-/-}$ MEFs were from D. Chan (California Institute of Technology, USA) and cultured as described previously[61]. SV40-transformed *Opa1*$^{-/-}$ and wild-type MEFs were a gift from C. Alexander (Max-Delbrück-Center for Molecular Medicine, Berlin, Germany) and cultured as described previously[32]. SV40-transformed wild-type and *Drp1*$^{-/-}$ MEFs were from K. Mihara (Tokyo Medical and Dental University, Japan) and cultured as previously described[34]. Wild-type and *Bax*$^{-/-}$*Bak*$^{-/-}$ MEFs were cultured as described previously[62]. Transfection of MEFs with DNA was carried out using Transfectin (Biorad), with siRNA using Oligofectamine (Invitrogen) according to the manufacturer's instructions. When indicated, cells were transfected with siRNA 24 h after seeding on glass coverslips and with mtYFP 48 h after plating. HeLa, HepG2 and C2C12 cells were gifts from C. Montecucco, A. Alberti and M. Sandri (University of Padova, Italy) and were cultured in Dulbecco's Modified Eagle Medium (DMEM, Invitrogen) supplemented with 10% fetal bovine serum (FBS, Invitrogen), 2 mM L-glutamine, non-essential amino acids (0.89 g l^{-1} L-alanine, 1.32 g l^{-1} L-asparagine, 1.33 g l^{-1} L-aspartic acid, 1.47 g l^{-1} L-glutamic acid, 0.75 g l^{-1} glycine, 1.15 g l^{-1} L-proline and 1.05 g l^{-1} L-serine, Invitrogen), 75 U ml^{-1} penicillin and 50 μg ml^{-1} streptomycin (Invitrogen) at 37 °C in a 5% CO_2 atmosphere. Transfection with siRNAs and DNA was carried out with Lipofectamine 2000 (Invitrogen) according to the manufacturer's protocol.

Primary hepatocytes were isolated as described previously[63] and cultured in DMEM (Invitrogen) supplemented with 10% FBS (Invitrogen), 1 nM insulin (Sigma), 2 mM L-glutamine, non-essential amino acids (Invitrogen), 75 U ml^{-1} penicillin, 50 μg ml^{-1} streptomycin (Invitrogen) and Fungizone (Invitrogen) at 37 °C in a 5% CO_2 atmosphere.

To trigger starvation, cells were washed four times and then incubated in Hanks balanced salt solution (HBSS) supplemented with 10 mM HEPES at pH 7.4, at 37 °C for the indicated time.

Fasting. Animal studies were carried out in compliance with local animal welfare regulations. CD1 mice were fasted for 12 h with free access to water.

Imaging. For confocal microscopy imaging of live cells, 1.8×10^5 cells seeded onto 24-mm round glass coverslips transfected and treated as indicated were placed on the stage of a Nikon Eclipse TE300 inverted microscope equipped with a PerkinElmer Ultraview LCI confocal system, a piezoelectric *z*-axis motorized stage (Pifoc, Physik Instrumente) and an Orca ER 12-bit CCD (charge-coupled device) camera (Hamamatsu Photonics). Cells expressing mtYFP or mtRFP were excited using the 488 nm or the 543 nm line of a HeNe laser (PerkinElmer) with a ×60, 1.4 NA Plan Apo objective (Nikon).

For quantification of the mitochondrial fusion rate, 2×10^5 cells seeded onto 24-mm round glass coverslips were co-transfected with mtRFP and mito-pAGFP. After 24 h, cells were treated as indicated and placed on the stage of a laser scanning microscope (TCS SP5, Leica). Using the LasAF software (Leica), regions of interest to be photoactivated were manually defined. To activate the pAGFP fluorescence, 1 *z* plane was activated using 100% of the power of the 413 nm laser line with a ×63, 1.4 NA objective. Frames were then acquired each minute using the 488 nm and the 563 laser lines for 30 min. Standard deviation of the green fluorescence in the whole cell was measured and normalized for the intensity of the mtRFP fluorescence using the Multi Measure plug-in of ImageJ (NIH).

For FRET imaging, 2×10^5 MEFs seeded onto 24-mm round glass coverslips were transfected with EPACI–camps and after 24 h placed on a thermostatically controlled chamber at 37 °C and maintained in complete medium on the stage of an Olympus inverted microscope equipped with a CellR imaging system and a beam-splitter optical device (Multispec Microimager; Optical Insights). Sequential images of the 545 nm fluorescence emission on excitation at 430 and 480 nm were acquired every second with a ×40, 1.4 NA objective (Olympus) using the CellR software and then processed using the Multi Measure plug-in of Image J (NIH) following background subtraction and expressed as FRET 430/480 ratio.

Real-time imaging of the mitochondrial membrane potential was carried out on 1×10^5 MEFs seeded onto 24-mm round glass coverslips and loaded with TMRM, using the Olympus CellR imaging system. Imaging and analysis of TMRM fluorescence over mitochondrial regions of interest was carried out as described previously[62].

Immunofluorescence microscopy. Primary hepatocytes were seeded onto 13-mm round glass coverslips coated with laminin. After 48 h, cells were treated as indicated and fixed for 30 min at room temperature with 3.7% (w/v) formaldehyde, permeabilized for 20 min with ice-cold Nonidet P40 (GIBCO) and incubated with rabbit anti-TOM20 (1:200, Santa Cruz Biotechnology). Staining was revealed with goat anti-rabbit IgG conjugated to fluorescein isothiocyanate (FITC) using a Nikon Eclipse TE300 inverted confocal microscope and a ×60, 1.4 NA Plan Apo objective (Nikon). Stacks of 50 images separated by 0.2 μm along the *z* axis were acquired. Three-dimensional reconstruction and volume rendering of the stacks were carried out with the appropriate plug-in of ImageJ (NIH).

Electron microscopy. MEFs of the indicated genotypes and treated as indicated were fixed with 1.25% (v/v) glutaraldehyde in 0.1 M sodium cacodylate at pH 7.4 for 1 h at room temperature. Muscle and liver specimens from mice treated as indicated were fixed in 2% formaldehyde, 2.5% (v/v) glutaraldehyde in 0.1 M sodium cacodylate at pH 7.4 for 2 h at room temperature and then overnight at 4 °C. Electron microscopy was carried out as described previously[10].

Morphometric and co-localization analysis. Morphometric analysis of mitochondrial shape was carried out as described previously[2]. For morphometric analysis of cristae biogenesis, mitochondria were randomly selected from coded samples and the number of cristae was counted and normalized for the surface of the organelle calculated by fitting a region of interest on the selected organelle using the Multi Measure plug-in of Image J (NIH). Co-localization between autophagosomes and mitochondria was quantified using Manders' coefficient[30].

Isolation of mitochondria. Cells plated in 500 cm^2 plates were treated after 48 h as indicated and mitochondria were isolated as described previously[64]. Protein concentration was determined by Bradford analysis.

Cell lysis. Cells (10^6) were collected and disrupted in Triton X-100 lysis buffer (1% Triton X-100, 150 mM NaCl and 50 mM Tris, at pH 7.4) in the presence of complete protease-inhibitor cocktail (Sigma) and phosphatase inhibitor cocktail 1 (Sigma). Protein concentration was determined by BCA assay (Pierce).

Immunoprecipitation. For immunoprecipitation, 150 μg of total cellular extract was dissolved in Triton X-100 lysis buffer and pre-cleared by centrifugation at 14,000*g*. A 50μl volume of dynabeads (Invitrogen) conjugated with protein-G was incubated with anti-DRP1 (1:50, BD Transduction) for 2 h at room temperature. Following three washes, cleared extracts were added and incubated overnight at 4 °C. Beads were washed three times and boiled in NuPage loading buffer (Invitrogen).

Immunoblotting. The indicated amounts of proteins were separated by 4–12% Bis-Tris, 12% Bis-Tris or 7% Tris-acetate gels (NuPAGE, Invitrogen) and transferred onto polyvinylidene difluoride (PVDF, BioRad) membranes. The following antibodies were used: anti-OPA1 (1:1,000, BD Transduction), anti-MFN1 (1:1,000, Abcam), anti-MFN2 (1:1,000, Abcam), anti-DRP1 (1:1,000, BD Transduction), anti-Fis1 (1:1,000, Alexis), anti-actin (1:30,000, Chemicon), anti-TOM20 (1:5,000, Santa Cruz Biotechnology), anti-phospho-Ser637-DRP1 (ref. 5; 1:1,000), anti-phospho-CREB-Ser133 (1:1,000, Cell Signalling), anti-CREB (1:1,000, Cell Signalling), anti-β-tubulin (1:200, Santa Cruz Biotechnology), anti-cyclophilin-D, anti-MnSOD (1:5,000, Stressgen), anti-complex-II, subunit 70 M_r (K) (1:1,000, MitoSciences), anti-PMP70 (1:1,000, Sigma), anti-ATPase, α subunit (1:1,000, MitoSciences), anti-mTOR (1:1,000, Cell Signalling), anti-LC3 (1:200, Anaspec) and anti-p62 (1:5,000, Progen).

Blue-native polyacrylamide gel electrophoresis. Cells (500 μg) were resuspended in 50 μl of native loading buffer (Invitrogen) containing 4% digitonin (Sigma) and protease-inhibitor cocktail (Sigma). After 30 min at 4 °C, the lysate was spun at 22,000*g* for 30 min at 4 °C. A 4 μl volume of native additive G250 5% (Invitrogen) was added to the supernatant and 30 μg of protein was loaded onto a 3–12% native gel (Invitrogen). Transfer of native gels was carried out as described above.

In-gel ATPase activity assay. ATPase activity was measured according to ref. 65 and ATPase activity was followed for up to 4 h at room temperature. Gels were washed in water to stop the reaction.

ATP measurement. Total ATP levels were measured by chemiluminescence using the ATP detection assay system ATPlite (PerkinElmer), according to the manufacturer's protocol. ATP levels were normalized by total protein concentration.

DOI: 10.1038/ncb2220

To measure mitochondrial ATP levels during starvation, cells grown on 13-mm round glass coverslips at 50% confluence were transfected with mitochondrially targeted luciferase and after 24 h luminescence was measured as described previously[35]. Basal luminescence was recorded in the absence of luciferin and then cells were perfused with 20 μM luciferin to record mitochondrial luminescence, which was then calibrated to the maximal luminescence emitted by the mitochondrially targeted luciferase by perfusing each sample with 10 mM ATP in the presence of 100 μM digitonin.

Flow cytometry. For analysis of cell death, 4×10^4 MEFs of the indicated genotype grown in 12-well plates were treated as indicated 24 h after seeding. When indicated, cells were collected and stained with propidium iodide and annexin-V-FLUOS (BenderMedSystems) according to the manufacturer's protocol. Cell viability was measured by flow cytometry (FACSCalibur, BD Biosciences) as the percentage of annexin-V- and propidium-iodide-negative events.

For evaluation of membrane potential, 4×10^4 MEFs of the indicated genotype were grown in 12-well plates and indicated treatments (starvation) were started 36 h after seeding. At the indicated times, cells were collected, washed with PBS, resuspended in HBSS supplemented with 10 mM HEPES at pH 7.4 and loaded with 20 nM TMRM (Molecular Probes) in the presence of 2 mg ml^{-1} cyclosporine H, a P-glycoprotein inhibitor, for 30 min at 37 °C. Cells were then analysed by flow cytometry (FACSCalibur, BD Biosciences).

Statistical tests. In each graph, unless noted, data represent mean ± s.e.m. of the indicated number (n) of independent experiments. If indicated, statistical significance has been calculated by a two-tailed Student t-test between the indicated samples. P values are indicated in the legends.

60. Nikolaev, V. O., Bünemann, M., Hein, L., Hannawacker, A. & Lohse, M. J. Novel single chain cAMP sensors for receptor-induced signal propagation. *J. Biol. Chem.* **279,** 37215–37218 (2004).
61. de Brito, O. M. & Scorrano, L. Mitofusin 2 tethers endoplasmic reticulum to mitochondria. *Nature* **456,** 605–610 (2008).
62. Scorrano, L. *et al.* BAX and BAK regulation of endoplasmic reticulum Ca^{2+}: a control point for apoptosis. *Science* **300,** 135–139 (2003).
63. Danial, N. N. *et al.* BAD and glucokinase reside in a mitochondrial complex that integrates glycolysis and apoptosis. *Nature* **424,** 952–956 (2003).
64. Frezza, C., Cipolat, S. & Scorrano, L. Organelle isolation: functional mitochondria from mouse liver, muscle and cultured fibroblasts. *Nat. Protoc.* **2,** 287–295 (2007).
65. Alirol, E. *et al.* The mitochondrial fission protein hFis1 requires the endoplasmic reticulum gateway to induce apoptosis. *Mol. Biol. Cell* **17,** 4593–4605 (2006).

nature cell biology

DOI: 10.1038/ncb2220

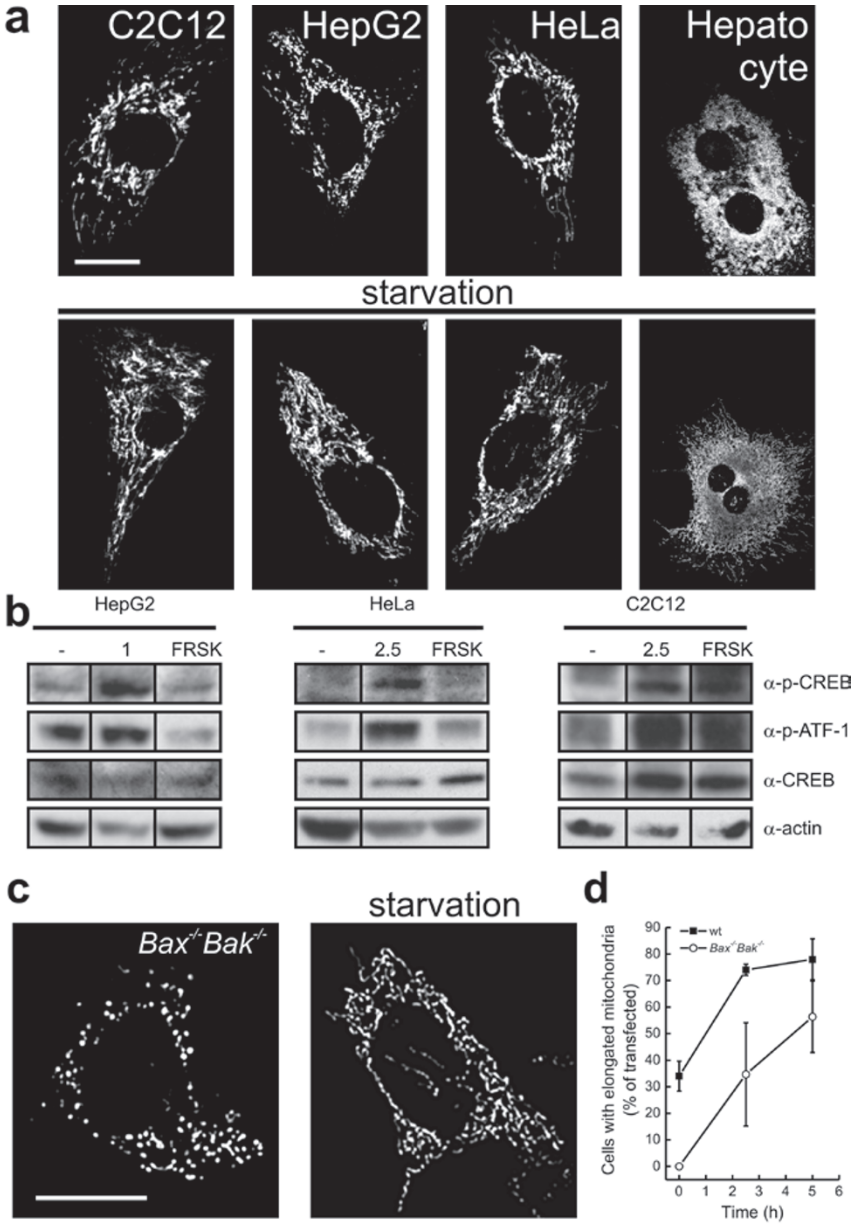

Figure S1 Starvation induces mitochondrial elongation and PKA activation in different cell lines. **(a)** Representative images of mitochondrial morphology. C2C12, HeLa and HepG2 cells were transfected with mtYFP and after 24 hrs imaged. Primary hepatocytes were fixed and immunostained for TOM20. Where indicated, cells were starved for 2.5 hrs. Bar, 20 μm. **(b)** Fifty μg of proteins of the indicated cells were separated by SDS-PAGE and immunoblotted with the indicated antibodies. Where indicated, cells were starved for 2.5 hrs or treated with 25 μM forskolin (FRSK) for 30 min. **(c)** Representative images of mitochondrial morphology in *Bax*$^{-/-}$*Bak*$^{-/-}$ MEFs. MEFs were transfected with mtYFP and imaged 24 hrs after by confocal microscopy. Where indicated, cells were starved. Bar, 20 μm. **(d)** Morphometric analysis of mitochondrial shape in *Bax*$^{-/-}$*Bak*$^{-/-}$ and the relative wt MEFs. Experiments were carried exactly as in (c). Data represent mean ± SEM of 5 independent experiments. In each experiment 50 cells were scored per condition.

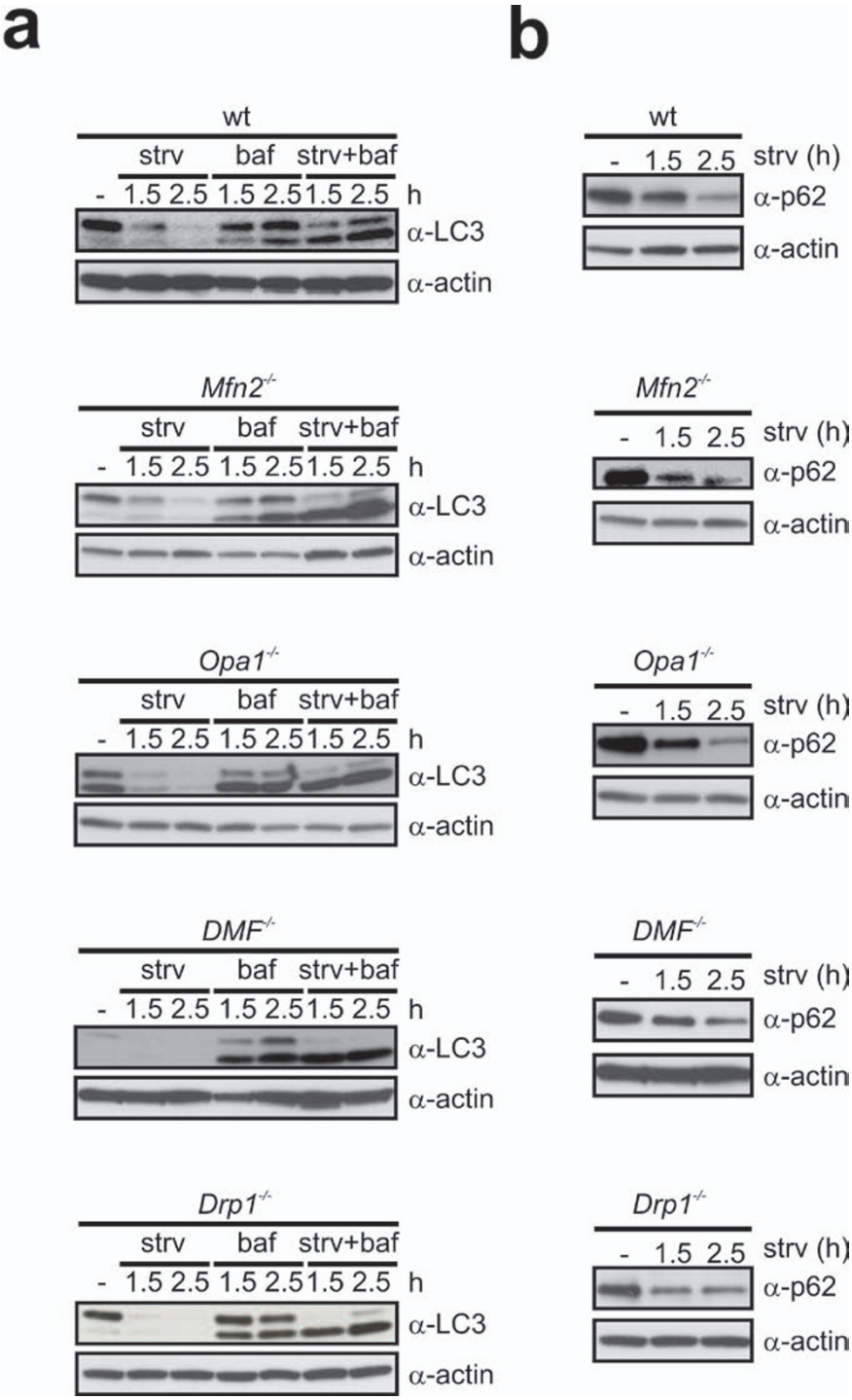

Figure S2 Autophagic flux is not affected in fusion-deficient MEFs. **(a-b)** Twenty μg of lysates of MEFs of the indicated genotypes were separated by SDS-PAGE and immunoblotted with the indicated antibodies. In (a) where indicated, MEFs were starved for the indicated periods and treated with 200 nM Bafilomycin A1 (baf). In (b) cells were starved for the indicated times.

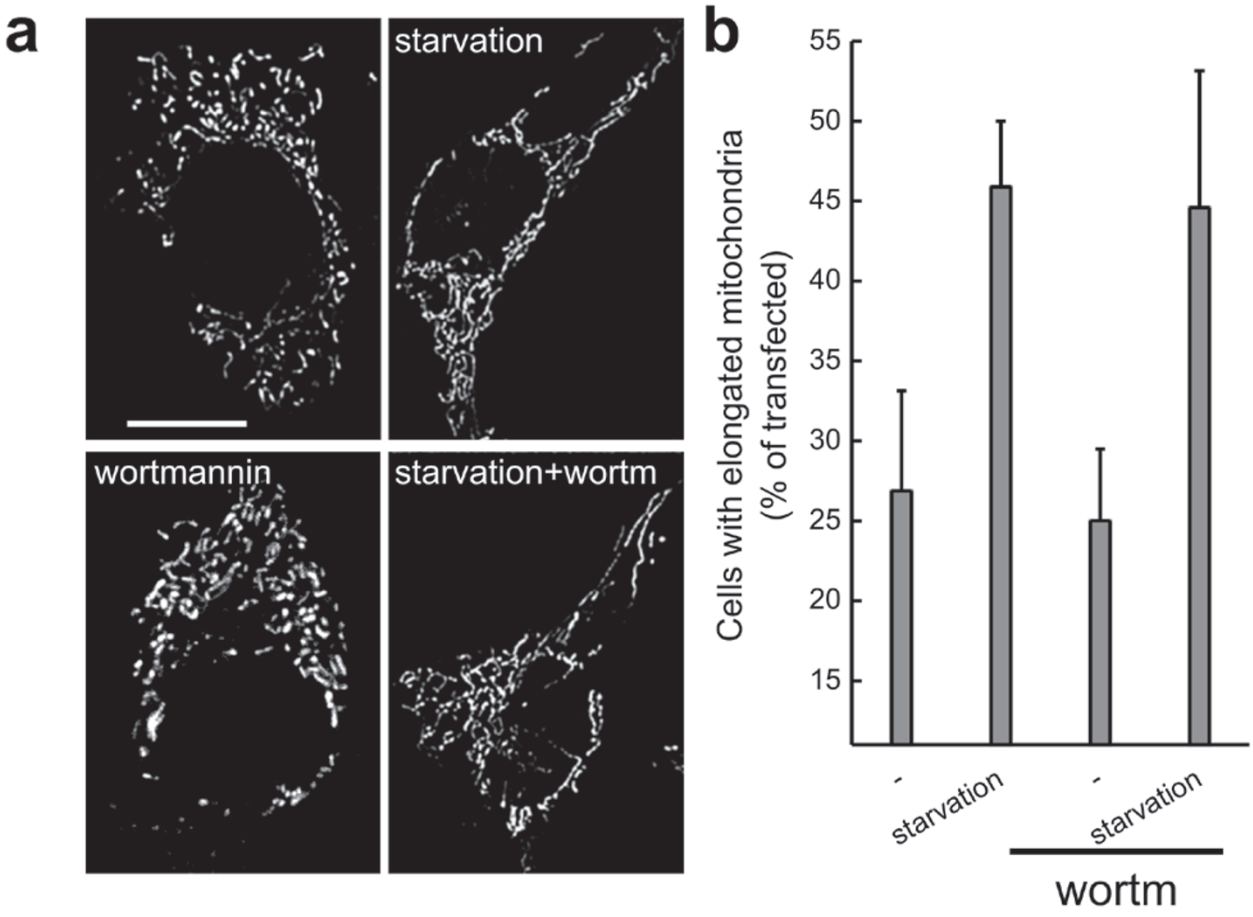

Figure S3 Blockage of autophagosome formation does not inhibit mitochondrial elongation in response to starvation. **(a)** Representative images of mitochondrial morphology. MEFs were transfected with mtYFP and after 24 hrs confocal images were acquired. Where indicated, cells were starved for 2.5 hrs and treated with 0.5 μM wortmannin. Bar, 20 μm. **(b)** Morphometric analysis of mitochondrial shape. Experiments were carried exactly as in (a). Data represent mean ± SEM of 5 independent experiments. In each experiment 50 cells were scored per condition.

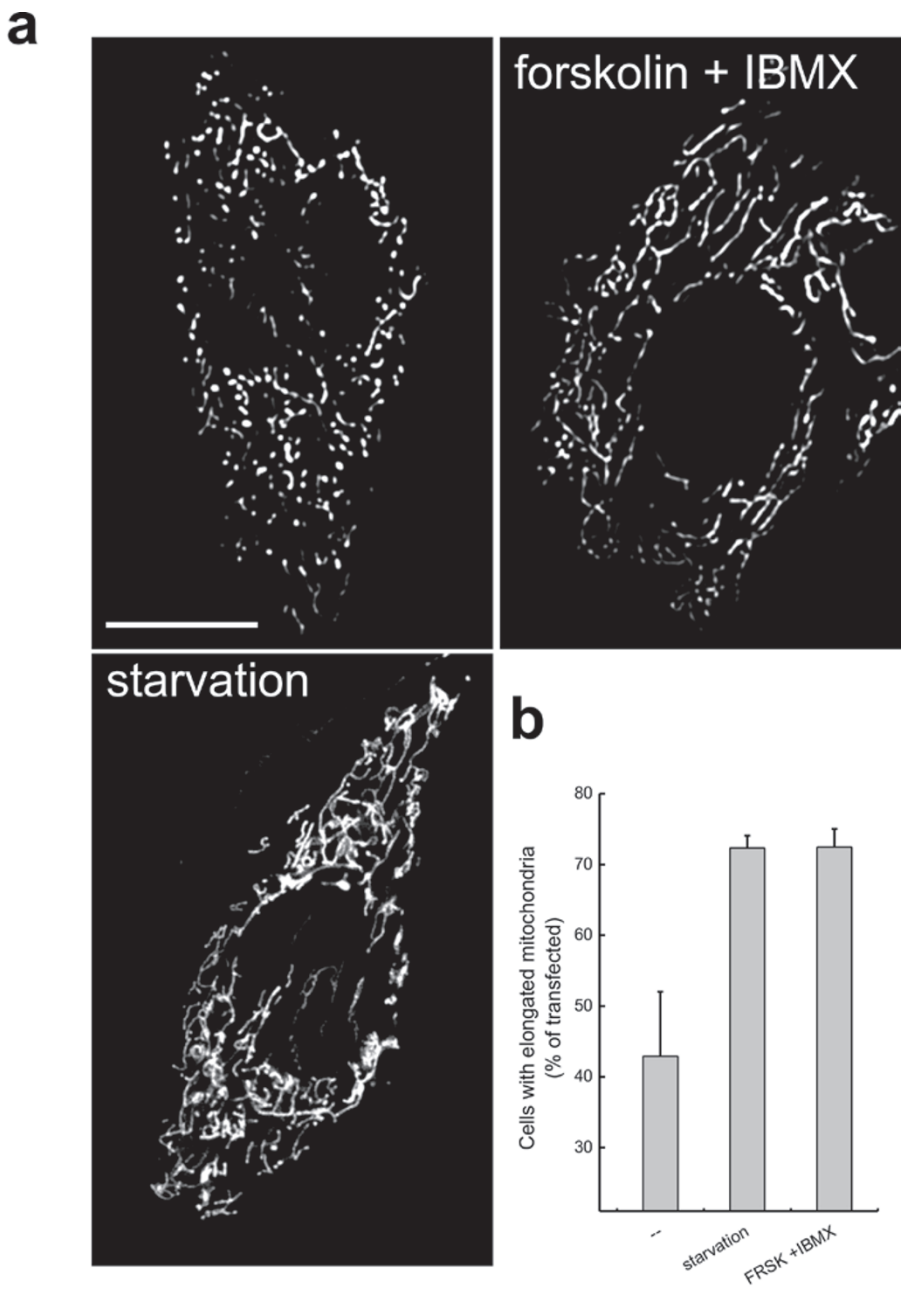

Figure S4 Pharmacological PKA activation leads to mitochondrial elongation. **(a)** Representative images of mitochondrial morphology. MEFs were transfected with mtYFP and after 24 hrs imaged by confocal microscopy. Where indicated, cells were starved for 2.5 hrs or treated with forskolin (FRSK) plus IBMX for 30 min. Bar, 20 μm. **(b)** Morphometric analysis of mitochondrial shape. Experiments were carried exactly as in (a). Data represent mean ± SEM of 5 independent experiments. In each experiment 50 cells were scored per condition.

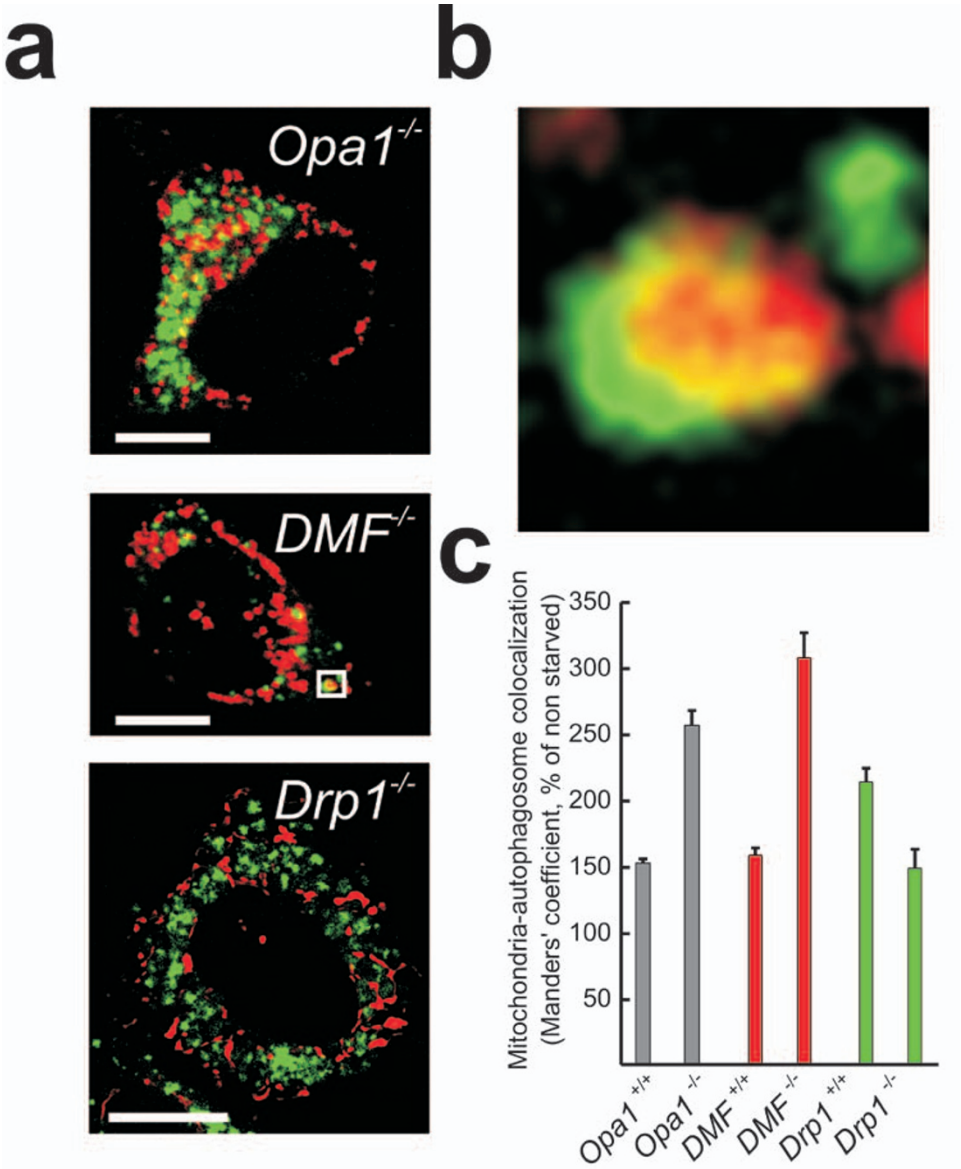

Figure S5 Increased colocalization of mitochondria with autophagosomes upon starvation of fusion-incompetent MEFs. **(a)** Representative images of mitochondria and autophagosomes. MEFs of the indicated genotype were starved 24 hrs after transfection with mtRFP and YFP-LC3 for 5 hrs in the presence of 200 nM Bafilomycin A1, fixed and imaged by confocal microscopy. Bars, 20 μm. **(b)** Magnification (10X) of the white box in (a) showing the engulfment of a fragmented mitochondrion by an LC3-positive autophagosome. **(c)** Quantitative analysis of mitochondria-autophagosome colocalization. Experiments were carried exactly as in (**a**). Data were normalized to the Manders' coefficient in non starved cells and they represent mean ± SEM of 5 independent experiments. In each experiment 50 cells were scored per condition.

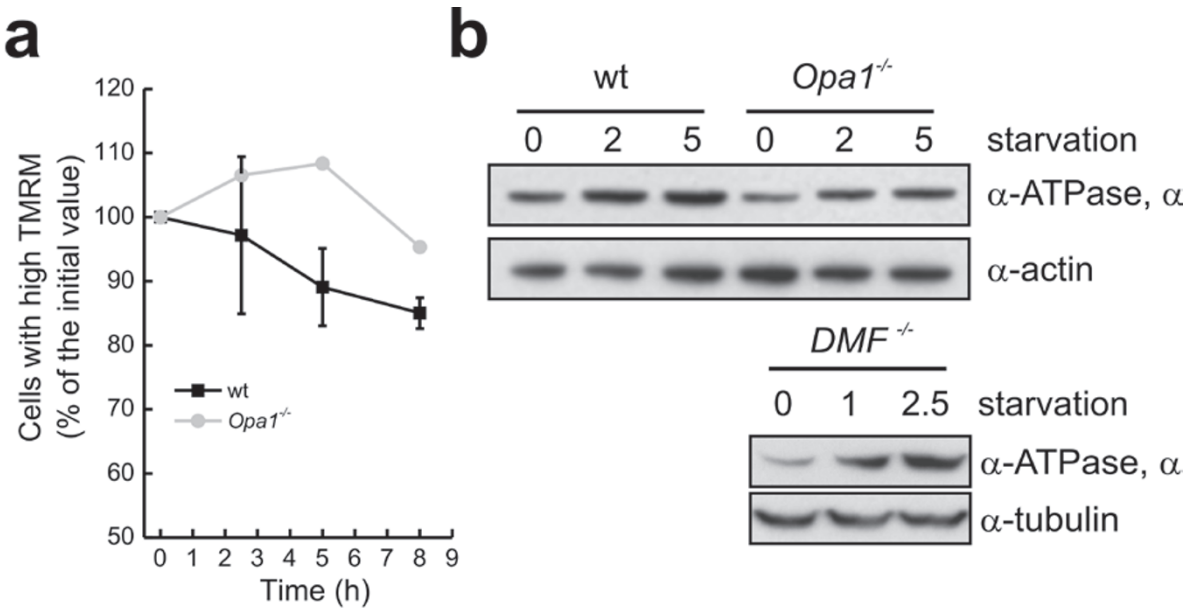

Figure S6 Mitochondrial membrane potential and ATPase levels during starvation. **(a)** Flow cytometric analysis of TMRM uptake during starvation**.** MEFs of the indicated genotype were starved for the indicated periods of time, harvested and stained with TMRM. Uptake of TMRM was determined by flow cytometry. Data represent the mean ± SEM of 5 independent experiments. **(b)** Mitochondrial ATPase levels during starvation. Twenty five μg of lysates of MEFs of the indicated genotypes were analyzed by SDS-PAGE/immunoblotting using the indicated antibodies. Where indicated, MEFs were starved for the indicated periods.

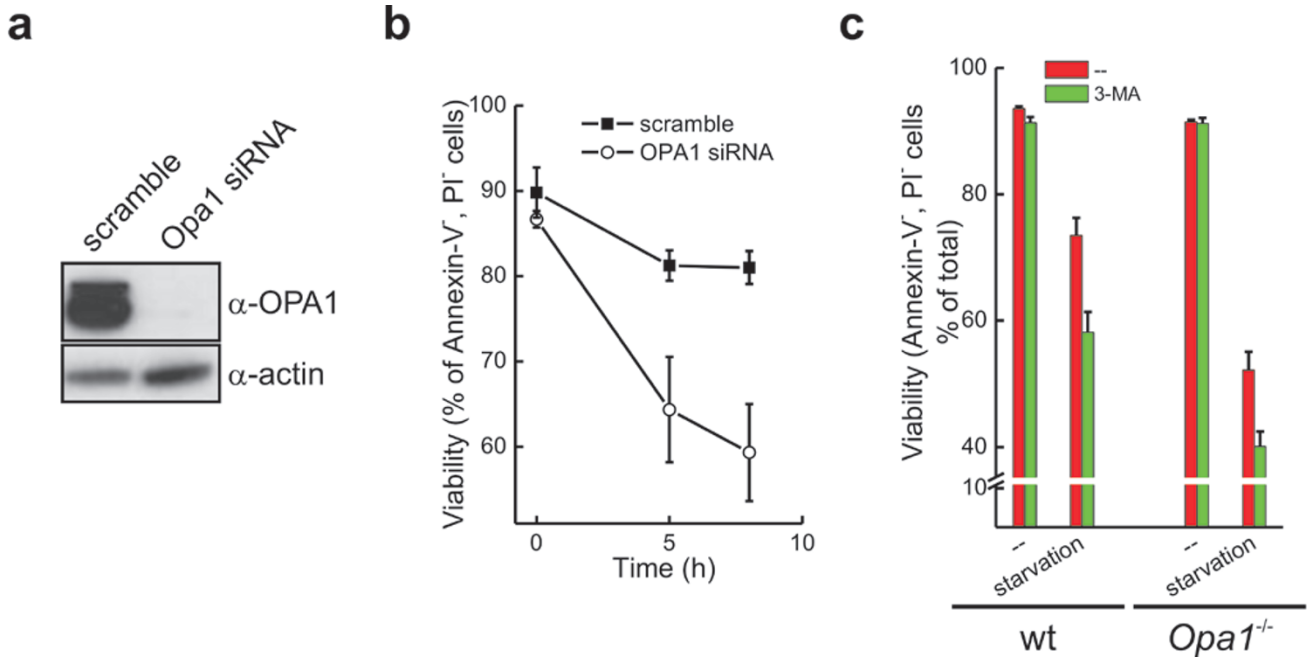

Figure S7 Starvation-induced cell death is accelerated by downregulation of *OPA1* or by inhibition of autophagy. **(a)** HeLa cells were transfected with the indicated siRNA and after 48 hrs lysed and 25 µg of proteins were separated by SDS-PAGE and immunoblotted with the indicated antibodies. **(b)** At the indicated times after starvation, cells were harvested and viability was determined by flow cytometry. Data represent mean ± SEM of 3 independent experiments. **(c)** Cells of the indicated genotype were starved for 5 hrs, harvested and viability was determined by flow cytometry. Where indicated, cells were treated with 10mM 3-MA. Data represent mean ± SEM of 7 independent experiments.

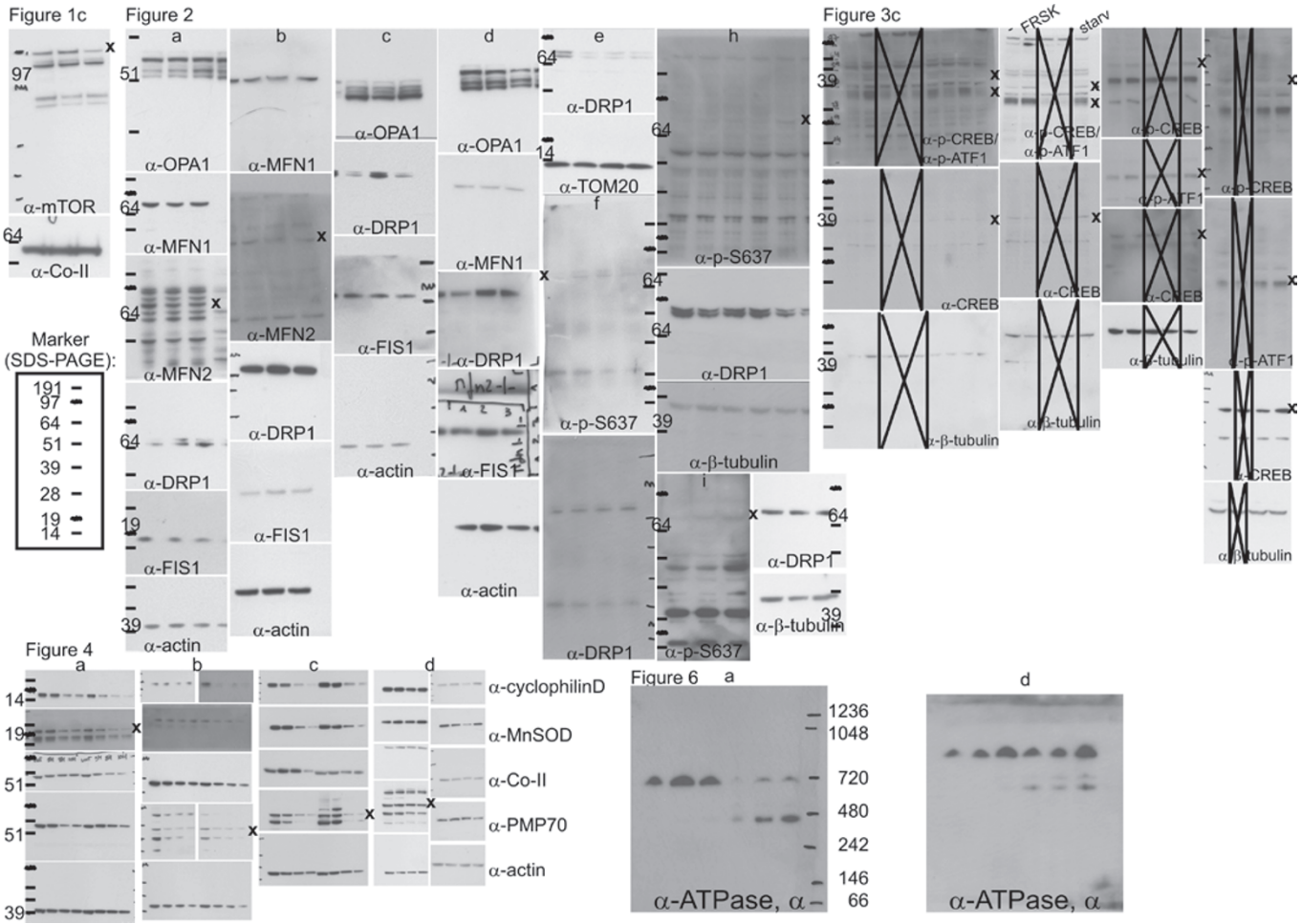

Figure S8 Full scans of key Western blot data. In many experiments, membranes were cut prior to probing each strip with a separate antibody. When unspecific bands are present, the band that corresponds to the molecular weight of the protein probed is indicated by an (x). Crossed lanes represent lanes that were cut out from the Western-blots in the main figures where this has been indicated by vertical bars. The orientation of the samples is the same as in the main figures except when specified.

Supplementary Movie Legends

Movie S1 Real time imaging of mito-pAGFP diffusion in wt MEFs. MEFs were cotransfected with mtRFP and mito-pAGFP. After 24 hrs mito-pAGFP was photoactivated in a ROI of fixed dimension as described and real time images of GFP and RFP fluorescence were acquired each min as described. The movie shows a composite image of GFP (green) and RFP (red) fluorescence.

Movie S2 Real time imaging of mito-pAGFP diffusion in starved wt MEFs. The experiment is exactly as in Movie S1, except that cells were starved for 2.5 hrs.

Movie S3 Real time FRET imaging demonstrate an increase in cAMP levels during starvation. MEFs transfected with Epac-CI. After 24 hrs real time imaging of Epac-CI FRET was performed as described. The movie shows the pseudocolor-coded FRET ratio of Epac-CI (red, higher, blue, lower FRET). Where indicated, cells were perfused with the starvation medium or with Forskolin+IBMX.